P. TOMASSINI[1,2,✉]
A. GIULIETTI[1,2]
D. GIULIETTI[1,2,3]
L.A. GIZZI[1,2]

Thomson backscattering X-rays from ultra-relativistic electron bunches and temporally shaped laser pulses

[1] Intense Laser Irradiation Laboratory, IPCF CNR, Via Moruzzi 1, 56124 Pisa, Italy
[2] INFN Section of Pisa, sq. B. Pontecorvo, 56127 Pisa, Italy
[3] Department of Physics 'E. Fermi', University of Pisa, sq. B. Pontecorvo, 56127 Pisa, Italy

ABSTRACT The process of Thomson scattering of an ultra-intense laser pulse by a relativistic electron bunch has been proposed as a way to obtain a bright source of short, tunable and quasi-monochromatic X-ray pulses. The real applicability of such a method depends crucially on the electron-beam quality, the angular and energetic distributions playing a relevant role. In this paper we present the computation of the Thomson-scattered radiation generated by a plane-wave, linearly polarized and flat-top laser pulse, incident on a counterpropagating electron bunch having a sizable angular divergence and a generic energy distribution. Both linear and nonlinear Thomson-scattering regimes are considered and the impact of the rising front of the pulse on the scattered-radiation distribution has been taken into account. Simplified relations valid for long laser pulses and small values of both scattering angle and bunch divergence are also reported. Finally, we apply the results to the cases of backscattering with electron bunches typically produced with both standard radio-frequency-based accelerators and laser–plasma accelerators.

PACS 13.60.Fz; 41.60.-m; 41.75.Jv

1 Introduction

Thomson scattering from free electrons is a pure electrodynamical process in which each particle radiates while interacting with an electromagnetic wave. From the quantum-mechanical point of view Thomson scattering is a limiting case of the process of emission of a photon by an electron absorbing one or more photons from an external field (see e.g. [1] and references therein), in which the energy of the scattered radiation is negligible with respect to the electron's energy. If the particle absorbs only one photon from the field (the *linear* or *nonrelativistic quivering* regime), Thomson scattering is the limit of Compton scattering in which the wavelength λ_X of the scattered photon observed in the particle's rest frame is

much larger than the Compton wavelength $\lambda_c = h/m_e c$ of the electron [2]. Since $\lambda_c/\lambda_X \ll 1$, the Thomson-scattering process can be fully described within classical electrodynamics both in the linear and the *nonlinear* (i.e. when the electron absorbs more than one photon) regimes.

Thomson scattering of a laser pulse by energetic counter-propagating electrons has been proposed since 1963 [3–5] as a quasi-monochromatic and polarized photon source. With the development of ultra-intense chirped and pulsed amplification (CPA) laser systems [6], the interest in this process dramatically renewed. The Thomson-scattering process of photons of ultra-intense laser pulses onto relativistic electron bunches can be employed as a bright source of energetic photons from UV to γ rays [7–9], an attosecond source in the full nonlinear regime [10], powerful diagnostics on the bunch itself [11–14] and a bunch cooler [15].

Recent experimental investigations [16–20] performed in the linear regime confirmed the production of a high-brightness X-ray flux in 90° and 180° collisions between CPA laser pulses and ultra-relativistic bunches; several proposals for direct medical applications of these sources have been presented [21–24].

The four main parameters of the Thomson-scattering process of a pulse by a free electron are the particle energy $E_0 = \gamma_0 m_e c^2$, the laser pulse peak normalized amplitude $a_0 \equiv e^2 A/(m_e c^2) = 8.5 \times 10^{-10}\sqrt{I\lambda_0^2}$, I being the peak intensity in W/cm² and λ_0 the wavelength in μm, the pulse longitudinal envelope rise time T_R and the angle α_L between the propagation directions of the pulse and the electron. The pulse amplitude a_0 controls the momentum transferred from the laser pulse to the electron, i.e. the number of photons of the pulse absorbed by the electron. If $a_0 \ll 1$, only one photon is absorbed and the resulting electron motion always admits a reference frame in which the quivering is nonrelativistic (linear Thomson scattering). For an electron initially moving with $\gamma_0 \gg 1$ and a pulse having an adiabatic rising front (i.e. with a rise time T_R much greater than the pulse period λ_0/c), the resulting scattered radiation is spectrally shifted at a peak wavelength $\lambda_X \simeq \lambda_0/(2\gamma_0^2(1 - \cos\alpha_L))$ and emitted forward with respect to the electron initial motion within a cone of aperture $\approx 1/\gamma_0$.

✉ Fax: +39-050-315-2256, E-mail: tomassini@ipcf.cnr.it

In the nonlinear regime ($a_0 \approx 1$ or higher) the resulting strong exchange between the laser pulse and the particle momentum induces a complex and relativistic electron motion, consisting of a drift and a quivering having both longitudinal and transverse components with respect to the pulse propagation. In turn, the time-dependent longitudinal drifting results in a nonharmonic electron motion, thus producing scattered radiation with a complex spectral distribution too. If the electron interacts with a laser pulse with constant amplitude, the spectral distribution of the scattered radiation is organized in equally spaced harmonics. This appealing feature requires at least that the laser pulse must be temporally 'shaped' in a flat-top way. Pulse-shaping techniques are becoming more common, especially for the production of ultra-short and low-emittance electron bunches with radio-frequency (RF) guns [25]. Moreover, the shaping of the laser pulse enables the occurrence of a quite subtle mechanism, which has been recently pointed out by He, Lau, Umstadter, Kowalczyk and Strickler. The authors of [26–28] showed that, for a pulse having a sharp flat-top envelope ($cT_R/\lambda_0 \to 0$), the value of the phase of the electric field at the rising front plays a relevant role for the particle dynamics and thus for the scattered-radiation distribution.

In this paper we develop an analytical estimation of the distribution of the photons radiated by Thomson scattering in both linear and nonlinear regimes by a free electron moving against a linearly polarized laser pulse. Several simplified expressions which are valid for the cases of small scattering angles or long pulses are also reported. We consider both the cases of *sharp* flat-top ($cT_R/\lambda_0 \to 0$) and *smooth* flat-top ($1 < cT_R/\lambda_0 \ll T/\lambda_0$) pulses, by taking into account the effect of the pulse rising front accordingly. Moreover, unlike the work of Esarey et al. [7], in our formalism the electrons need not experience perfect head-on collisions with the laser pulse photons but they can have an incidence angle small enough to enable the transverse ponderomotive forces to be neglected and large enough to produce a sizable effect on the scattered distribution itself. We stress also that the formula for the radiated distribution we report here differs from that proposed by Ride et al. [29] in two respects: (i) ours takes into account the effects of the rising front of the pulse and (ii) it can be directly applied to the estimation of the scattered-radiation distribution by an electron bunch, e.g. by means of a Monte Carlo computation.

The paper is organized as follows. In Sect. 2 Thomson (quasi) backscattering by a single electron will be considered and an exact analytical expression of the scattered-radiation distribution for the case of a linearly polarized, flat-top and radially homogeneous laser pulse is deduced. Several simplified relations which are valid for the cases of long pulse and small scattering and incidence angles, and *both* long pulse and small angles, are also reported. The case of linear Thomson scattering will also be discussed and the validity of the approximations of negligible effects of the transverse ponderomotive forces for the realistic case of a Gaussian transverse profile will be clearly stated. In Sect. 3 we deal with Thomson backscattering by an electron bunch presenting sizable angular divergence and arbitrary energy distribution. Both collective and coherence effects are neglected. For the linear-regime case and the case of ultra-relativistic electrons and small scatter-

ing and incidence angles, we compare the expression for the scattered-radiation distribution to the simple relation found in the literature [8]. Next, we specialize to the production of energetic and quasi-monochromatic photons and we systematically study the effect of the beam angular divergence on the spectrum of the scattered radiation in both the linear and the nonlinear regimes. Section 4 is devoted to comments.

2   Single-electron scattering for a linearly polarized flat-top pulse

2.1   *The vector potential for a flat-top-shaped pulse*

Let us consider a plane-wave laser pulse linearly polarized along the y axis propagating along the $-z$ direction, having wavelength λ_0, duration T and transverse size of waist w_0. The pulse electric field is parameterized as $\vec{E}(z, t) = E_0 \hat{y} H(\xi) \sin(\omega_0 \xi + \phi_0)$, where $\xi \equiv t + z/c$, $\omega_0 = 2\pi c/\lambda_0$ is the laser pulsation, E_0 is the pulse amplitude, $H(\xi)$ is a flat-top longitudinal profile (see Fig. 1) and ϕ_0 is the phase of the electromagnetic wave at the rising front located at $\xi = 0$. We introduce the adimensionalized vector potential of the laser pulse $\vec{a} \equiv (e^2/m_e c^2)\vec{A}$, which in the Coulomb gauge ($\vec{\nabla} \cdot \vec{a} = 0$) can be parameterized as

$$\vec{a}(z, t) \equiv \hat{y} a(\xi) = -\hat{y} a_0 \omega_0 \int_{-\infty}^{t} d\tau H(\tau + z/c)$$
$$\times \sin(\omega_0(\tau + z/c) + \phi_0). \quad (1)$$

The longitudinal envelope for the *sharp* flat-top case (i.e. with rising time scale $T_R \ll \lambda_0/c$) is $H(x) = \Theta(x) - \Theta(x - T)$, $\Theta(x)$ being the Heaviside step function. For this case the pulse vector potential is easily computed with Eq. (1), giving

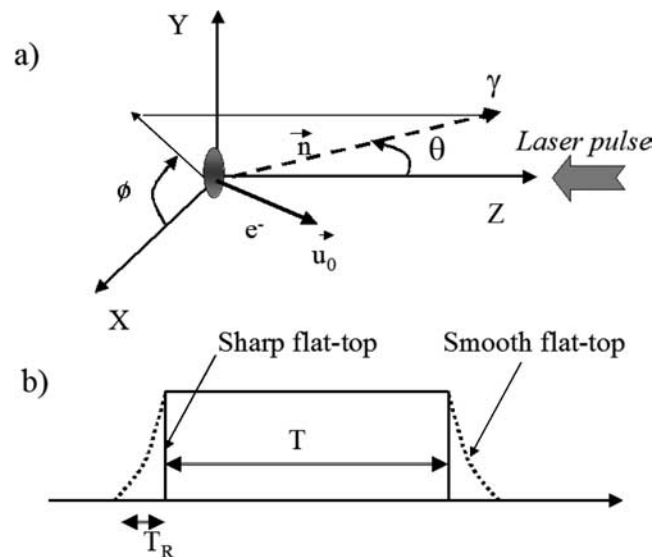$$a(\xi) = a_0 H(\xi)(\cos(\omega_0 \xi + \phi_0) - \cos(\phi_0)) \quad \text{[sharp profile]}.$$

FIGURE 1   a Geometry of Thomson backscattering. The laser pulse is polarized along y and moves towards negative $z's$. Each electron moves roughly along positive $z's$ with initial momentum $m_e c \vec{u}_0$. The scattered radiation is collected along the direction $\vec{n}$ with angles (θ, ϕ). **b** Longitudinal envelope profile of the pulse for both the sharp flat-top and the smooth flat-top cases
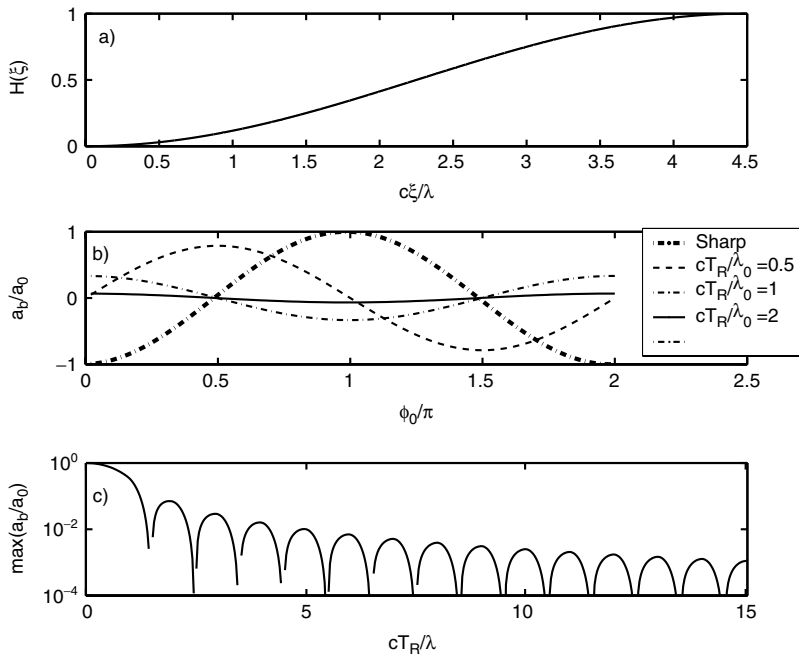
FIGURE 2 **a** Time shape of the pulse rising front $H(\xi) = \sin(\pi\xi/2T_R)$ for the case $L_R = 15\,\text{fs}$. **b** Initial phase dependence of the mean potential $\bar{a}(\phi_0)$ for some values of the rising time scales. **c** Dependence of the maximum of $\bar{a}(\phi_0)$ on the rising time scale

We immediately note that for this sharp limiting case the mean value over a pulse cycle of the vector potential $\bar{a} = -a_0 \cos(\phi_0)$ is generally not null, so that the initial phase plays a relevant role in the particle dynamics as stated in [26–28]. The sharp flat-top profile, however, is to date far from being really obtained and for present-time applications the most realistic case of a smooth flat-top profile should be considered instead. The smooth flat-top profile has rising and falling fronts having scales cT_R larger than the pulse wavelength λ_0 and much smaller than the pulse duration T (see Fig. 1b). The integration of Eq. (1) for a smooth longitudinal profile brings us generally to a vector potential having a complex analytical description. Such a detailed description, however, is not necessary since $T_R/T \ll 1$ and thus the scattered radiation emission during the rising (and falling) front is negligible with respect to that of the plateau. Nevertheless, the value of the ratio cT_R/λ_0 plays a key role in determining the dynamics of the particle in the plateau region ($H(\xi) = 1$ for $\xi \geq T_R$), since the mean value of the vector potential in the plateau $\bar{a}$ (and thus that of the transverse particle momentum, as will be clear below) depends on the rising front shape. In order to better highlight this, let us write the value of the vector potential in the plateau region as

$$a(\xi) = a_0 \cos(\omega_0 \xi + \phi_0) + \bar{a}, \qquad (2)$$

where

$$\bar{a} = -a_0 \left[\cos(\omega_0 T_R + \phi_0) + \omega_0 \int_0^{T_R} \mathrm{d}\tau\, H(\tau) \sin(\omega_0 \tau + \phi_0) \right] \qquad (3)$$

and where we have supposed that $H(0) = 0$ and $H(\xi) = 1$ for $\xi \geq T_R$. The mean potential $\bar{a}$ is an oscillating function of the initial phase ϕ_0 with period 2π. Note that if H is a regular function also in the interval $0 < \xi < T_R$ with $cT_R \gg \lambda_0$, the amplitude of $\bar{a}(\phi_0)$ can be estimated by making an iterative integration by parts of Eq. (3), obtaining a series of terms proportional

to $\partial^n H/\partial \xi^n$ computed in both $\xi = 0$ and $\xi = T$. As a result, for $\lambda_0/(cT_R) \gg 1$, $\bar{a}$ is roughly of the order $\mathcal{O}(a_0[\lambda_0/(cT_R)]^n)$ with $n \geq 1$. As an example, we consider the case of a rising front of the shape $H(\xi) = \sin^2(\pi\xi/(2T_R))$ for $0 \leq \xi \leq T_R$. In Fig. 2a the shape of $H(\xi)$ for the case $T_R = 15\,\text{fs}$ and $\lambda_0 = 1\,\mu\text{m}$ is shown. We computed the initial phase dependence of $\bar{a}$ for several values of the rising front time scale T_R, obtaining the curves reported in Fig. 2b. Finally, in Fig. 2c the dependence of the maximum of $\bar{a}(\phi_0)$ on the rising time scale is reported, confirming that $\bar{a}/a_0 = \mathcal{O}(\lambda_0/cT_R)^2$.

2.2   *Single-particle dynamics in the pulse plateau region*

In the following we will describe the dynamics of the particles *in the plateau region*. This will be accomplished by taking into account the mean value $\bar{a}$ of the vector potential. Let us introduce the normalized electron momentum $\vec{u}(t) = \vec{p}(t)/mc = \gamma(t)\vec{\beta}(t)$, γ being the relativistic Lorentz factor, and the initial normalized momentum $\vec{u}_0 = \vec{p}_0/mc = \gamma_0\vec{\beta}_0$. Since space-charge forces are neglected, the Lagrangian of each electron can be written as

$$\mathcal{L} = -\sqrt{1 - \vec{\beta}^2(t)} - \vec{\beta}(t) \cdot \vec{a}(z(t), t) \qquad (4)$$

and the invariance of the Lagrangian (4) under translations orthogonal to z generates two conservation rules for the transverse component of the generalized momentum $\vec{P}(t) \equiv \vec{u} + \vec{a}$. Moreover, the total time derivative of the Hamiltonian $\mathcal{H} \equiv \vec{P} \cdot \vec{\beta} - \mathcal{L}$ is linked to the *partial* time derivative of the Lagrangian: $\mathrm{d}\mathcal{H}/\mathrm{d}t = -\partial\mathcal{L}/\partial t$. As a result, the time and space invariance properties of $\mathcal{L}$ generate three conservation laws, by which the time evolution of the particle momentum can be inferred:

$$\frac{\mathrm{d}}{\mathrm{d}t} u_x = 0, \quad \frac{\mathrm{d}}{\mathrm{d}t}(u_y - a) = 0, \quad \frac{\mathrm{d}}{\mathrm{d}t}(\gamma + u_z) = 0, \qquad (5)$$

where $\gamma(t) = (1 + \vec{u}^2(t))^{1/2}$ is the Lorentz factor of the particle. Let us consider a particle with initial momentum $\vec{u}_0 = (u_{x0}, u_{y0}, u_{z0})$. The solution of Eq. (5) is (see also [7] for the special case of $u_{x0} = u_{y0} + \bar{a} = 0$)

$$u_x = u_{x0}, \quad u_y = u_{y0} + a, \quad u_z + \gamma = h_0, \tag{6}$$

where $h_0 \equiv \gamma_0 + u_{z0}$, $\vec{u}_\perp^2 \equiv u_x^2 + u_y^2 = u_{x0}^2 + (u_{y0} + a)^2$ and $\gamma = (h_0^2 + 1 + \vec{u}_\perp^2)/2h_0$. In the plateau region the mean value over a pulse cycle of the particle momentum reads

$$\begin{aligned} \bar{u}_x &= u_{x0}, \quad \bar{u}_y = (u_{y0} + \bar{a}), \\ \bar{u}_z &= \left[h_0^2 - \left(1 + u_{x0}^2 + (u_{y0} + \bar{a})^2 + a_0^2/2\right)\right]/(2h_0), \end{aligned} \tag{7}$$

so that the longitudinal particle speed in the plateau $\beta_z^{\mathrm{L}} = \bar{u}_z/\bar{\gamma}$ is

$$\beta_z^{\mathrm{L}} = \frac{\left[h_0^2 - \left(1 + u_{x0}^2 + (u_{y0} + \bar{a})^2 + a_0^2/2\right)\right]}{\left[h_0^2 + \left(1 + u_{x0}^2 + (u_{y0} + \bar{a})^2 + a_0^2/2\right)\right]}. \tag{8}$$

We note that, for an ultra-relativistic electron ($\gamma_0 \gg 1$) and the case $|u_{y0} + \bar{a}| \ll u_{z0}$, the mean longitudinal speed can be simplified as

$$\beta_z^{\mathrm{L}} \simeq \frac{1 - a_0^2/8\gamma_0^2}{1 + a_0^2/8\gamma_0^2}. \tag{9}$$

It is interesting to note that both the transverse and the longitudinal components of the mean momentum differ from their initial values: the longitudinal ponderomotive forces of the pulse rising front do reduce the mean longitudinal momentum and the mean momentum along the pulse polarization is changed by the electric field during the rising front. As a result, the mean particle momentum inside the pulse plateau makes an angle $\bar{\theta}$ with respect to the z axis satisfying

$$\tan \bar{\theta} = \frac{\bar{u}_\perp}{\bar{u}_z} = \frac{2h_0 \left(u_{x0}^2 + (u_{y0} + \bar{a})^2\right)}{\left[h_0^2 - \left(1 + u_{x0}^2 + (u_{y0} + \bar{a})^2 + a_0^2/2\right)\right]}. \tag{10}$$

We stress that such an incidence angle may differ considerably from the incidence angle $\theta_0 = \tan^{-1}(u_{\perp 0}/u_{z0})$ that the particle had *before* it reached the pulse. This implies that, due to both the acquired transverse momentum and the reduced longitudinal momentum, the particles can escape the inner region of the pulse focal spot even if their unperturbed trajectories were very close to the pulse-propagation axis. This effect has been already stressed for the sharp-plateau case [27].

The computation of the particle trajectory is strongly simplified by expressing its position as a function of the parameter $\xi \equiv t + z(t)/c$. Introducing the ξ derivative of the position $\tilde{\vec{\beta}} \equiv \mathrm{d}\vec{r}/c\mathrm{d}\xi = \vec{\beta}/(1 + \beta_z)$, we obtain

$$\tilde{\beta}_x = \frac{u_{x0}}{h_0}, \quad \tilde{\beta}_y = \frac{u_{y0} + a}{h_0}, \quad \tilde{\beta}_z = \frac{h_0^2 - (1 + \vec{u}_\perp^2)}{2h_0^2}, \tag{11}$$

and the parametric description of the particle position *in the plateau* can be obtained by integrating Eq. (11) over the ξ parameter.

After the introduction of both the auxiliary vector $\vec{v} \equiv \vec{u}_0 + \bar{a}\hat{y}$ and the parameter $\tilde{h}_0^2 \equiv [h_0^2 - (1 + \vec{v}_\perp^2 + 1/2a_0^2)]$

and having omitted inessential constant terms, we found

$$x(\xi)/c = \frac{v_x}{h_0}(\xi - \xi_0),$$

$$y(\xi)/c = \frac{v_y}{h_0}(\xi - \xi_0) + \frac{a_0}{\omega_0 h_0} \sin(\omega_0(\xi - \xi_0)), \tag{12}$$

$$\begin{aligned} z(\xi)/c = &\frac{\tilde{h}_0^2}{2h_0^2}(\xi - \xi_0) - \frac{a_0 v_y}{\omega_0 h_0^2} \sin(\omega_0(\xi - \xi_0)) \\ &- \frac{a_0^2}{8\omega_0 h_0^2} \sin(2\omega_0(\xi - \xi_0)), \end{aligned}$$

where $\xi_0 = -\phi_0/\omega_0$. The auxiliary vector $\vec{v}$ can be interpreted as follows. Consider a particle p_1 with initial momentum $\vec{u}_0$ interacting with a pulse characterized by a given $\bar{a}$. The vector $\vec{v}$ represents the initial momentum which a particle p_2 should have if we impose that (i) its dynamics in the plateau is the same as p_1 and (ii) it interacts with a pulse with $\bar{a} = 0$, i.e. with a mean transverse momentum $\bar{u}_y = v_y$. It is therefore convenient to introduce the particle incidence angles in the spherical coordinate system (θ_e, ϕ_e) by defining them in terms of $\vec{v}$ instead of $\vec{u}_0$:

$$\vec{v} = v \left(\sin \theta_e \cos \phi_e, \sin \theta_e \sin \phi_e, \cos \theta_e \right).$$

We stress that the particle incidence angles (θ_e, ϕ_e) are referred to the effective initial momentum $\vec{v}$ and *not* to the mean particle momentum in the pulse plateau $\bar{u}$.

2.3   *Thomson-scattered radiation by a single particle*

In the classical description of the interaction of an electron with an electromagnetic wave, the distribution of the scattered radiation can be obtained by computing the retarded potentials associated with the accelerated electrons [31]. Such a description is valid provided that the energy E_{X} of the scattered photons is much lower than the electron energy [2]. In the far-field approximation, the distribution of the scattered photons emitted with pulsation ω along the direction $\vec{n}$ (see Fig. 1a) can be obtained with the relation [31]

$$\frac{\mathrm{d}^2 N}{\mathrm{d}\Omega \mathrm{d}\omega} = \frac{\alpha}{(2\pi)^2} \omega \left| \int \mathrm{d}t\, \vec{n} \times (\vec{n} \times \vec{\beta}(t)) \mathrm{e}^{i\omega(t - \vec{n} \cdot \vec{r}(t)/c)} \right|^2, \tag{13}$$

where $\alpha = e^2/\hbar c$ is the fine-structure constant, $\vec{\beta} \equiv \mathrm{d}\vec{r}/c\mathrm{d}t$ is the electron speed and $\mathrm{d}\Omega$ is the unit solid angle.

The time integral in Eq. (13) can be estimated analytically provided that several assumptions are fulfilled. First, the collective space-charge effects are negligible, i.e. each electron oscillates independently of the others. This assumption is valid for short enough pulses, as reported in [7], and it has been used to derive the particle's momentum during the interaction. Second, the pulse Rayleigh length $Z_{\mathrm{R}} = \pi w_0^2/\lambda_0$ is much larger than the pulse longitudinal size cT, so that the plane-wave approximation holds. Third, the initial radial position r_0 of each electron should be smaller than the pulse transverse size w_0 *and* the electron incidence angle θ_e satisfies $|\theta_e| < 2(w_0 \beta_z^{\mathrm{L}}/cT)$. In this case each electron of the bunch lies in the region in which the radial distance from the pulse axis is smaller than the pulse transverse size *for all the duration* $t_{\mathrm{int}} = T/(1 + \beta_z^{\mathrm{L}}) \simeq T[1 + a_0^2/8\gamma_0^2]/2$ *of the interaction.*

For a usual Gaussian transverse envelope, this assumption enables the approximation that each electron interacts with a radially homogeneous plane wave, thus allowing us to neglect the transverse ponderomotive forces (for an *a posteriori* discussion of the validity of the approximation see Sect. 2.8).

By using relations (6) and (12), the exponential term in Eq. (13) can be written as

$$\exp\left[i\omega\left(t - \frac{\vec{n} \cdot \vec{r}}{c}\right)\right] \equiv \exp\left[i(\Psi_0 + \delta\Psi)\right], \tag{14}$$

where

$$\delta\Psi = \omega\left(\rho_0(\xi - \xi_0) - \rho_1 \frac{1}{\omega_0} \sin\omega_0(\xi - \xi_0)\right.$$
$$\left. + \rho_2 \frac{1}{\omega_0} \sin 2\omega_0(\xi - \xi_0)\right),$$

$$\rho_0 = \frac{1}{h_0^2}\left[h_0^2 - \frac{(1 + \cos\theta)}{2}\tilde{h}_0^2 - h_0 \sin\theta(v_x \cos\phi + v_y \sin\phi)\right],$$

$$\rho_1 = \frac{a_0}{h_0^2}[h_0 \sin\theta \sin\phi - v_y(1 + \cos\theta)],$$

$$\rho_2 = \frac{a_0^2}{8h_0^2}(1 + \cos\theta) \tag{15}$$

and Ψ_0 an inessential phase factor which can be omitted since an incoherent summation over the single-particle contributions is employed.

Following Ref. [7], the computation of the scattered-radiation distribution proceeds by decomposing the term $\vec{n} \times (\vec{n} \times \vec{\beta})$ in Eq. (13) as a sum of a vector parallel to the versors $\hat{\theta}$ and $\hat{\phi}$ of the spherical coordinates

$$\vec{n} \times (\vec{n} \times \vec{\beta}) = -\hat{\theta}(\tilde{\beta}_x \cos\theta \cos\phi + \tilde{\beta}_y \cos\theta \sin\phi - \tilde{\beta}_z \sin\theta)$$
$$+ \hat{\phi}(\tilde{\beta}_x \sin\phi - \tilde{\beta}_y \cos\phi) \tag{16}$$

and by making an expansion of the exponential term with the help of the Bessel identity $\exp(i\mu \sin\phi) = \sum_{n=-\infty}^{\infty} J_n(\mu)\exp(in\phi)$. Moreover, defining the quantity

$$\vec{V} \equiv \frac{1}{T}\int_0^T d\xi \vec{n} \times (\vec{n} \times \vec{\beta}) \exp(i\delta\Psi) = \hat{\theta}V_\theta + \hat{\phi}V_\phi$$

and by using Eq. (15), the angular and spectral distribution of the radiation emitted by a *single* electron can be expressed as

$$\frac{d^2N}{d\Omega d\omega} = \frac{\alpha}{(2\pi)^2}\omega T^2(|V_\theta|^2 + |V_\phi|^2), \tag{17}$$

with

$$V_\theta = -\frac{1}{h_0}\sum_{m,n=-\infty}^{\infty} J_m\left(\rho_2\frac{\omega}{\omega_0}\right)e^{i\Delta\omega_n(T/2-\xi_0)}\operatorname{sinc}\left(\Delta\omega_n\frac{T}{2}\right)$$

$$\times \left\{\left[\cos\theta\cos\phi v_x + \cos\theta\sin\phi v_y - \sin\theta\tilde{h}_0^2\right]J_{n+2m}\right.$$

$$\times \left(\rho_1\frac{\omega}{\omega_0}\right) + a_0\left[\cos\theta\sin\phi + \sin\theta\frac{v_y}{4h_0}\right]$$

$$\times \left(J_{n+2m-1}\left(\rho_1\frac{\omega}{\omega_0}\right) + J_{n+2m+1}\left(\rho_1\frac{\omega}{\omega_0}\right)\right)$$

$$+ \sin\theta\frac{a_0^2}{8h_0}\left(J_{n+2m-2}\left(\rho_1\frac{\omega}{\omega_0}\right) + J_{n+2m+2}\left(\rho_1\frac{\omega}{\omega_0}\right)\right)\right\},$$

$$V_\phi = \frac{1}{h_0}\sum_{m,n=-\infty}^{\infty} J_m\left(\rho_2\frac{\omega}{\omega_0}\right)e^{i\Delta\omega_n(T/2-\xi_0)}\operatorname{sinc}\left(\Delta\omega_n\frac{T}{2}\right)$$

$$\times \left\{[\sin\phi v_x - \cos\phi v_y]J_{n+2m}\left(\rho_1\frac{\omega}{\omega_0}\right)\right.$$

$$\left. - \cos\phi\frac{1}{2}a_0\left(J_{n+2m-1}\left(\rho_1\frac{\omega}{\omega_0}\right) + J_{n+2m+1}\left(\rho_1\frac{\omega}{\omega_0}\right)\right)\right\}. \tag{18}$$

In Eq. (18) we have introduced $\Delta\omega_n \equiv \rho_0\omega - n\omega_0$ and $\operatorname{sinc}(x) \equiv \sin c(x)/x$. Equation (18) should be meant either as exact or approximate, depending of the real shape of the pulse. For a sharp flat-top pulse Eq. (18) is *exact* and the dependence of the scattered-radiation distribution on the initial phase is included having substituted the initial momentum u_{y0} with $u_{y0} - a_0 \cos\phi_0$. For a smooth flat-top profile Eq. (18) is *approximate* since the scattered radiation generated during the rising and falling fronts of the pulse has been neglected. Since for a smooth flat-top profile $\lambda_0/c \ll T_R \ll T$, the relative error introduced by truncating the time integration in Eq. (18) in the plateau region is of the order $T_R/T \ll 1$.

Each component of $\vec{V}$ is obtained as a sum of harmonics, each peaked at the resonance frequency $\omega_n = n\omega$ and having full width at half maximum $\delta\omega_n$, with

$$\omega_F = \frac{\omega_0}{\rho_0}, \quad \delta\omega_n \simeq \frac{1.2(2\pi)}{\rho_0 T} = \frac{1.2}{N_c}\omega_F \tag{19}$$

(see also Eq. (15)), N_c being the number of cycles of the laser pulse ($N_c = \omega_0 T/(2\pi)$). The relative spectral width ($\delta\omega_n/\omega_n$) of each harmonic in Eq. (18) reads

$$\frac{\delta\omega_n}{\omega_n} \simeq 1.2\frac{1}{nN_c}.$$

In the estimation of Eq. (17) we are faced with the square modulus of each V term, so in the general case the scattered photon spectral distribution is made up of a sum of products of harmonics of V_θ and V_ϕ with different harmonic numbers. Note, however, that a sensible overlapping between different harmonics can occur for very low pulse durations (namely $N_c < 2$, i.e. $T < 7$ fs for a $\lambda_0 = 1$-μm pulse).

Let us consider as an example the cases of an electron *moving exactly along the z direction* with $\gamma_0 = 10$ (i.e. of energy $\simeq 5$ MeV), colliding with two different *sharp* flat-top pulses of normalized amplitude $a_0 = 1.5$, wavelength $\lambda_0 = 1$ μm (i.e. of intensity $I \simeq 3 \times 10^{18}$ W/cm²) and different durations $T_1 = 3$ fs and $T_2 = 20$ fs, respectively. Both the pulses have an initial phase $\phi_0 = \pi/2$, so that the mean value of the vector potential is null. The computation of the scattered-photon distribution is obtained with Eqs. (17) and (18) and the results are sketched in Figs. 3 and 4, where the distributions in the plane $x = 0$ ($\phi = \pi/2$) are shown. In both the cases the scattered photons are emitted forward of the electron velocity into a cone of approximate aperture $\approx 1/\gamma_0$. However, the spectral distributions are very different: in the case of the 20-fs pulse a clear harmonic distribution is present (see also [7]), while in the case of 3 fs the regular distribution of equally
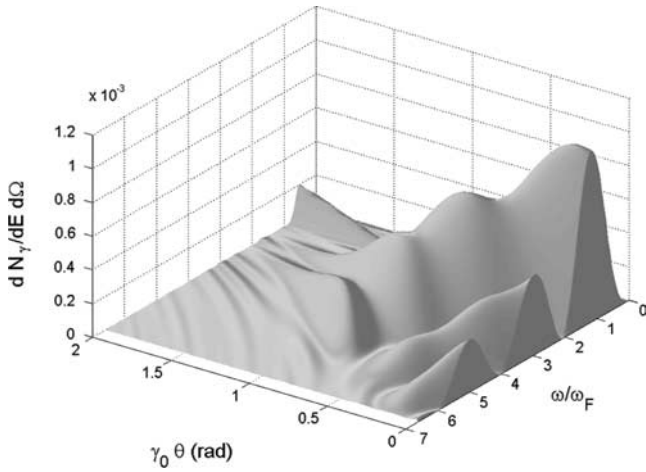
FIGURE 3 Spectral and angular distribution in arbitrary units of the photons emitted by the head-on collision between a 5-MeV electron ($\gamma_0 = 10$) moving along the z axis and a laser pulse of amplitude $a_0 = 1.5$, wavelength $\lambda_0 = 1\,\mu$m, duration $T_1 = 3$ fs and initial phase $\phi_0 = \pi/2$ ($\bar{a} = 0$). The radiation is collected at the azimuthal angle $\phi = \pi/2$ and is mainly emitted into a cone of aperture $\approx 1/\gamma_0$. The scattered-photon pulsation is shown in units of the fundamental frequency $\omega_F = \omega_0/\rho_0$ on the axis. Note that the spectral distribution does not resemble a sum of harmonics

spaced peaks is lost due to the overlapping between different n's in V_θ and V_ϕ.

If either $\bar{a} \neq 0$ or the electron is initially traveling *off axis*, the resulting scattered photons are distributed mainly into a cone whose axis is aligned with the vector $\vec{v}$ (see also [29], in which the effect of the initial phase was not taken into account). In order to make this more evident, let us consider the Thomson scattering between a laser pulse and an electron having the same parameters as the former example but where the direction of $\vec{v}$ is now *off axis* with incidence angle $\theta_e = 50$ mrad and azimuth angle $\phi_e = \pi/2$. Since $1/\gamma_0 \approx 0.1$, we expect that the radiation will be mainly emitted into a cone having direction ($\theta_e \approx 0.05$ rad, $\phi_e = \pi/2$ rad) in spherical coordinates, having an aperture $\approx 2/\gamma_0 \approx 0.2$ rad. The scattered radiation is then collected into a cone of half-

aperture $\theta_{\text{Max}} = 0.2$ rad aligned along the z axis and the resulting scattered-photon distribution in the plane $\phi = \pi/2$ is shown in Fig. 5.

2.4   *Small scattering angle approximation*

Usually the angular divergence of relativistic electron beams produced by standard RF accelerators is very low (values of the order of a few tens of milliradians are quite common) and electron beams obtained with novel acceleration schemes (e.g. laser–plasma accelerators) may have angular divergences of a few degrees as well [32, 33]. As stated before, the incidence angle of the particle in the pulse plateau θ_e depends on the $\bar{a}$ parameter too, so that in the following we will suppose that $v_y = u_{y0} + \bar{a}$ is negligible with respect to the longitudinal initial momentum $v_z = u_{z0}$; this is accomplished either by carefully tuning the initial phase for the sharp-plateau case or by using a pulse with a sufficiently high rising time. If a pulse with a very short rise time is employed, so that $\bar{a}$ is not very small with respect to u_{z0}, the small-angle approximation is valid provided that the electron bunch is initially moving off axis with $|u_{x0}| \ll u_{z0}$ and $|u_{y0} + \bar{a}| \ll u_{z0}$.

In the following we will suppose that each particle of the bunch is ultra relativistic ($\gamma_0 \gg 1$) and interacts with a pulse of amplitude $a_0 < \sqrt{8}\gamma_0$. In this case the scattered radiation is emitted mostly in a cone with aperture $\approx \sqrt{1 + a_0^2/2}/\gamma_0 \ll 1$ (see below). For these relativistic beams both incidence θ_e and scattering θ angles are small, so that a more simplified expression for the scattered-photon distribution can be found by making the following approximations: $\beta_0 \simeq 1 - 1/(2\gamma_0^2)$, $\sin\theta_e \simeq \theta_e$, $\cos\theta_e \simeq 1 - \theta_e^2/2$, $\sin\theta \simeq \theta$ and $\cos\theta \simeq 1 - \theta^2/2$ in Eq. (18), giving

$$V_\theta \simeq -\frac{1}{2\gamma_0} \sum_{m,n=-\infty}^{\infty} J_m\left(\rho_2 \frac{\omega}{\omega_0}\right) e^{i\Delta\omega_n(T/2-\xi_0)} \operatorname{sinc}\left(\Delta\omega_n \frac{T}{2}\right)$$

$$\times \left\{\left[\gamma\theta_e\cos(\phi-\phi_e)-\gamma\theta\left(1-\frac{a_0^2}{8\gamma_0^2}\right)\right] J_{n+2m}\left(\rho_1 \frac{\omega}{\omega_0}\right)\right.$$
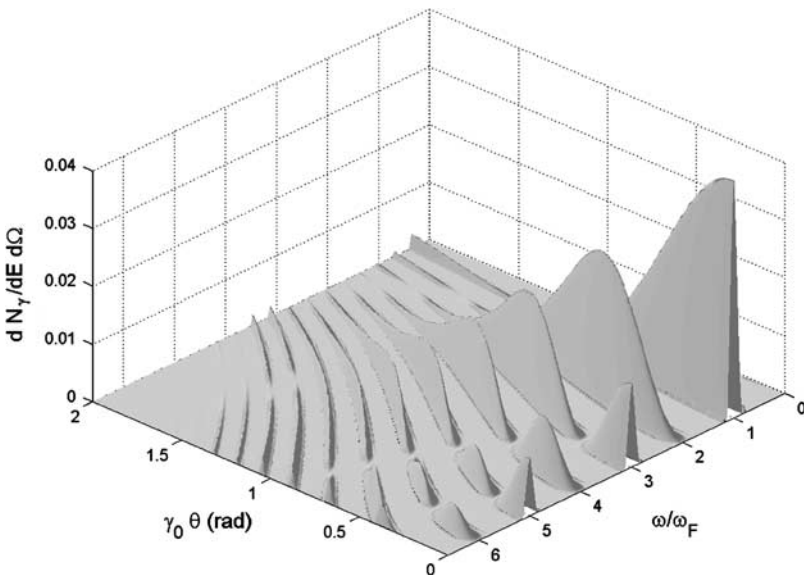

FIGURE 4 Spectral and angular distribution in arbitrary units of the photons emitted by the head-on collision between a 5-MeV electron ($\gamma_0 = 10$) moving along the z axis and a laser pulse of amplitude $a_0 = 1.5$, wavelength $\lambda_0 = 1\,\mu$m, duration $T_2 = 20$ fs and initial phase $\phi_0 = \pi/2$ ($\bar{a} = 0$). The radiation is collected at the azimuthal angle $\phi = \pi/2$ and the scattered-photon pulsation is shown in units of the fundamental frequency $\omega_F = \omega_0/\rho_0$ on the axis. Since $N_c = 6$, different harmonics are well separated
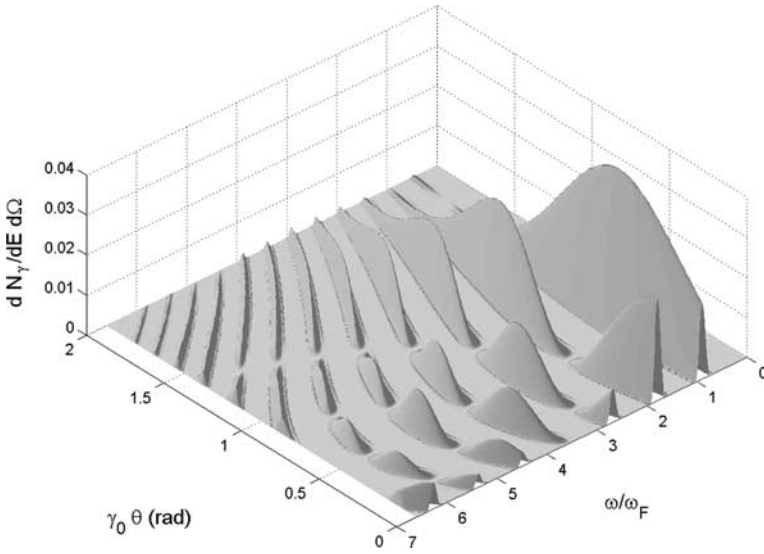
FIGURE 5 Spectral and angular distribution of the photons emitted by the head-on collision between a 5-MeV electron ($\gamma_0 = 10$) with an *off-axis* $\vec{v}$ vector ($\theta_e = 50$ mrad, $\phi_e = \pi/2$) and a laser pulse of amplitude $a_0 = 1.5$, wavelength $\lambda_0 = 1\,\mu$m and duration $T_2 = 20$ fs. The radiation is collected at the azimuthal angle $\phi = \pi/2$ and the scattered-photon pulsation is shown in units of the fundamental frequency $\omega_F = \omega_0/\rho_0$ at ($\theta = \theta_e, \phi = \phi_e$)

$$+ \left[\frac{1}{2}a_0 \sin\phi \right] \left(J_{n+2m-1}\left(\rho_1 \frac{\omega}{\omega_0} \right) + J_{n+2m+1}\left(\rho_1 \frac{\omega}{\omega_0} \right) \right)$$
$$+ \gamma_0\theta \frac{a_0^2}{16\gamma_0^2} \left(J_{n+2m-2}\left(\rho_1 \frac{\omega}{\omega_0} \right) + J_{n+2m+2}\left(\rho_1 \frac{\omega}{\omega_0} \right) \right) \Bigg\},$$

$$V_\phi \simeq \frac{1}{2\gamma_0} \sum_{m,n=-\infty}^{\infty} J_m\left(\rho_2 \frac{\omega}{\omega_0} \right) e^{i\Delta\omega_n(T/2-\xi_0)} \operatorname{sinc}\left(\Delta\omega_n \frac{T}{2} \right)$$
$$\times \left\{ \gamma_0\theta_e \sin(\phi - \phi_e) J_{n+2m}\left(\rho_1 \frac{\omega}{\omega_0} \right) - \cos\phi \frac{1}{2}a_0 \right.$$
$$\times \left. \left(J_{n+2m-1}\left(\rho_1 \frac{\omega}{\omega_0} \right) + J_{n+2m+1}\left(\rho_1 \frac{\omega}{\omega_0} \right) \right) \right\}, \quad (20)$$

where the following approximated relations for ρ_i are used:

$$\rho_0 \simeq \frac{1}{4\gamma_0^2} \left[1 + (\gamma_0\tilde{\theta})^2 + \frac{1}{2}a_0^2 \right],$$

$$\rho_1 \simeq \frac{a_0}{2\gamma_0^2} \left[\gamma_0\theta \sin\phi - \gamma_0\theta_e \sin\phi_e \right], \quad (21)$$

$$\rho_2 \simeq \frac{a_0^2}{16\gamma_0^2},$$

and where $\tilde{\theta} \equiv (\theta^2 + \theta_e^2 - 2\theta \cdot \theta_e \cos(\phi - \phi_e))^{1/2}$ is the angle between $\vec{v}$ and $\vec{n}$. In the small-angle limit the fundamental frequency ω_F reduces to

$$\omega_F = \frac{4\gamma_0^2}{\left[1 + (\gamma_0\tilde{\theta})^2 + \frac{1}{2}a_0^2 \right]} \omega_0. \quad (22)$$

For a given azimuthal angle ϕ the minimum value of $\tilde{\theta}$ is realized at the scattering angle

$$\theta_M = \theta_e \cos(|\phi - \phi_e|). \quad (23)$$

At this angle $\tilde{\theta}^2 = \theta_e^2 \sin^2(\phi - \phi_e)$ and the maximum value of the fundamental frequency at ϕ fixed reads

$$\omega_F^M = \frac{4\gamma_0^2}{\left[1 + (\gamma_0\theta_e \sin(\phi - \phi_e))^2 + \frac{1}{2}a_0^2 \right]} \omega_0. \quad (24)$$

The *absolute* maximum of ω_F is obtained with ($\theta = \theta_e$, $\phi = \phi_e$) (so that $\tilde{\theta} = 0$), i.e. when we observe the scattered photons in the same direction as the effective electron initial momentum $\vec{v}$ (see also [29]).

2.5   Long-pulse limit

Let us consider the case of a long laser pulse, i.e. a pulse with a large number of cycles $N_c \gg 1$. Since the width of each harmonic in Eq. (18) is much lower than the harmonic spacing $(\omega_{n+1} - \omega_n) = \omega_F$, the following approximations can be employed:

$$e^{i(\Delta\omega_n - \Delta\omega_m)(T/2-\xi_0)} \operatorname{sinc}(\Delta\omega_m T/2) \operatorname{sinc}(\Delta\omega_n T/2)$$
$$\simeq \delta_{mn} \operatorname{sinc}(\Delta\omega_n T/2)^2 J_m\left(\rho_2 \frac{\omega}{\omega_0} \right)$$
$$\simeq J_m(n\epsilon_2), \quad J_m\left(\rho_1 \frac{\omega}{\omega_0} \right) \simeq J_m(n\epsilon_1), \quad \text{for } \omega \simeq \omega_n, \quad (25)$$

where we have introduced the parameters

$$\epsilon_1 \equiv \frac{\rho_1}{\rho_0} = a_0 \frac{[h_0 \sin\theta \sin\phi - v_y(1 + \cos\theta)]}{\left[h_0^2 - \frac{(1+\cos\theta)}{2}\tilde{h}_0^2 - h_0 \sin\theta(v_x \cos\phi + v_y \sin\phi) \right]},$$

$$\epsilon_2 \equiv \frac{\rho_2}{\rho_0} = \frac{a_0^2}{8} \frac{(1 + \cos\theta)}{\left[h_0^2 - \frac{(1+\cos\theta)}{2}\tilde{h}_0^2 - h_0 \sin\theta(v_x \cos\phi + v_y \sin\phi) \right]},$$

$$(26)$$

and we have neglected the small dependence of the Bessel functions on their arguments within the spectral range of a single harmonic. This is justified provided that the combinations of parameters ϵ_1/N_c and ϵ_2/N_c are well below unity, because the error δJ introduced by approximating $J_m(\rho_{1,2}\omega/\omega_0)$ as $J_m(n\rho_{1,2}/\omega_0)$ is

$$\delta J_m \approx (\rho_{1,2}\delta\omega_n/\omega_0) J_m'(n\rho_{1,2}/\omega_0)$$
$$= (\epsilon_{1,2}/N_c)[J_{m-1}(n\epsilon_{1,2}) - J_{m+1}(n\epsilon_{1,2}/\omega_0)]/2.$$

As a result, the scattered-radiation distribution (Eq. (17)) can be approximated in the long-pulse limit as

$$\frac{d^2N}{d\Omega d\omega} \simeq \frac{\alpha}{(2\pi)^2}\omega T^2 \sum_{n=1}^{\infty} \left\{ \mathrm{sinc}^2\left(\Delta\omega_n \frac{T}{2}\right)(|\mathcal{C}_\theta(n,\theta,\phi)|^2 \right.$$

$$\left. + |\mathcal{C}_\phi(n,\theta,\phi)|^2) \right\}, \tag{27}$$

where

$$C_\theta(n,\theta,\phi) = -\frac{1}{h_0} \sum_{m=-\infty}^{\infty} J_m(n\epsilon_2)$$

$$\times \left\{ \left[\cos\theta\cos\phi v_x + \cos\theta\sin\phi v_y - \sin\theta\tilde{h}_0^2\right] \right.$$

$$\times J_{n+2m}(n\epsilon_1) + a_0\left[\cos\theta\sin\phi + \sin\theta\frac{v_y}{4h_0}\right]$$

$$\times (J_{n+2m-1}(n\epsilon_1) + J_{n+2m+1}(n\epsilon_1))$$

$$\left. + \sin\theta\frac{a_0^2}{8h_0}(J_{n+2m-2}(n\epsilon_1) + J_{n+2m+2}(n\epsilon_1)) \right\},$$

$$C_\phi(n,\theta,\phi) = \frac{1}{h_0} \sum_{m=-\infty}^{\infty} J_m(n\epsilon_2)\left\{ [\sin\phi v_x - \cos\phi v_y] \right.$$

$$\times J_{n+2m}(n\epsilon_1) - \cos\phi\frac{1}{2}a_0(J_{n+2m-1}(n\epsilon_1)$$

$$\left. + J_{n+2m+1}(n\epsilon_1)) \right\}. \tag{28}$$

For a given scattered direction, the radiation spectral distribution consists of a sum of equally spaced harmonics of a fundamental pulsation $\omega_F = \omega_0/\rho_0$. Since the natural line width of each harmonic is very small, it can be useful to express the spectral dependence of $d^2N/d\omega d\Omega$ by means of Dirac deltas. By using the limit $\sin(lx)^2/(lx^2) \to \pi\delta(x)$ for $l \to \infty$, the scattered-photon distribution can be further approximated as

$$\frac{d^2N}{d\Omega d\omega} \simeq \sum_{n=1}^{\infty} \mathcal{C}(n,\theta,\phi)\delta(\omega - n\omega_F), \tag{29}$$

where

$$\mathcal{C}(n,\theta,\phi) \equiv \alpha n\, N_c\frac{1}{\rho_0^2}(|\mathcal{C}_\theta(n,\theta,\phi)|^2 + |\mathcal{C}_\phi(n,\theta,\phi)|^2) \tag{30}$$

is the angular distribution of the scattered photons in the nth harmonic.

2.6   *Small scattering angle in the long-pulse (SALP) limit*

The long-pulse and small-angle approximations can be applied together for most of the Thomson backscattering experiments which can be performed nowadays, since the available ultra-intense laser pulses have durations exceeding tens of femtoseconds and usually ultra-relativistic electron bunches with reduced angular divergence are employed.

To get the SALP (small-angle, long-pulse) approximation of the scattered-photon distribution we start from the long-pulse limit (Eq. (27)) and we make the small-angle approximation in Eq. (28) supposing that $\theta \ll 1$, $\theta_e \ll 1$ and $\gamma_0 \gg 1$, giving

$$\mathcal{C}_\theta^{\mathrm{SALP}} \simeq -\frac{1}{2\gamma_0}\sum_{m=-\infty}^{\infty} J_m(n\epsilon_2)$$

$$\times \left\{ \left[\gamma\theta_e\cos(\phi-\phi_e) - \gamma\theta\left(1 - \frac{a_0^2}{8\gamma_0^2}\right)\right]J_{n+2m}(n\epsilon_1) \right.$$

$$+ \left[\frac{1}{2}a_0\sin\phi\right](J_{n+2m-1}(n\epsilon_1) + J_{n+2m+1}(n\epsilon_1))$$

$$\left. + \theta\frac{a_0^2}{16\gamma_0}(J_{n+2m-2}(n\epsilon_1) + J_{n+2m+2}(n\epsilon_1)) \right\}, \tag{31}$$

$$\mathcal{C}_\phi^{\mathrm{SALP}} \simeq \frac{1}{2\gamma_0}\sum_{m=-\infty}^{\infty} J_m(n\epsilon_2)$$

$$\times \left\{ \gamma_0\theta_e\sin(\phi-\phi_e)J_{n+2m}(n\epsilon_1) \right.$$

$$\left. - \cos\phi\frac{1}{2}a_0(J_{n+2m-1}(n\epsilon_1) + J_{n+2m+1}(n\epsilon_1)) \right\}.$$

In the SALP limit the ϵ_i parameters reduce to

$$\epsilon_1^{\mathrm{SALP}} \simeq 2a_0\frac{[\gamma_0\theta\sin\phi - \gamma_0\theta_e\sin\phi_e]}{[1 + (\gamma_0\tilde{\theta}^2)^2 + \frac{1}{2}a_0^2]},$$

$$\epsilon_2^{\mathrm{SALP}} \simeq \frac{1}{4}a_0^2\frac{1}{[1 + (\gamma_0\tilde{\theta}^2)^2 + \frac{1}{2}a_0^2]}. \tag{32}$$

We are able to obtain a simplified expression of Eq. (31), which is valid when we observe the scattered radiation in exactly the same direction as $\vec{v}$. When $(\theta = \theta_e, \phi = \phi_e)$ the ϵ_1 parameter is null, so that $J_q(p\epsilon_1) = \delta_{0,q}$. By using the relation $(J_{a-1}(x) + J_{a+1}(x)) = (2a/x)J_a(x)$, Eq. (31) reduces to

$$\mathcal{C}_\theta^{\mathrm{SALP}}(n,\theta_e,\phi_e) \simeq -\frac{1}{2\gamma_0}$$

$$\times \begin{cases} \frac{1}{4\gamma_0^2}\gamma_0\theta_e J_{-n/2}(n\epsilon_2) & n = \mathrm{even} \\[2mm] \frac{1}{2}a_0\sin\phi_e\left(J_{-(n-1)/2}(n\epsilon_2)\right. \\ \left. + J_{-(n+1)/2}(n\epsilon_2)\right) & n = \mathrm{odd} \end{cases} \tag{33}$$

$$\mathcal{C}_\phi^{\mathrm{SALP}}(n,\theta_e,\phi_e) \simeq -\frac{1}{2\gamma_0}$$

$$\times \begin{cases} 0 & n = \mathrm{even} \\[2mm] \frac{1}{2}a_0\cos\phi_e\left(J_{-(n-1)/2}(n\epsilon_2)\right. \\ \left. + J_{-(n+1)/2}(n\epsilon_2)\right) & n = \mathrm{odd} \end{cases}$$

Note that in $\mathcal{C}_\theta$ the even-harmonic term is negligible in the SALP approximation, so that the peak value of the nth odd

harmonic yield becomes

$$C(n, \theta_e, \phi_e) = \alpha n \, N_c \left(\frac{\gamma_0 a_0}{(1 + 1/2 \, a_0^2)} \right)^2$$

$$\times \left\{ \left[J_{-(n-1)/2} \left(n \frac{a_0^2}{4 + 2a_0^2} \right) \right. \right.$$

$$\left. \left. + \, J_{-(n+1)/2} \left(n \frac{a_0^2}{4 + 2a_0^2} \right) \right]^2 \right\}, \qquad (34)$$

while even-harmonic radiation is null. This result generalizes Eq. (39) in Ref. [7] for the case $\theta_i \neq 0$

2.7   *Linear Thomson scattering*

The nonrelativistic quivering limit can be derived by Eqs. (15), (17) and (18) by performing a perturbative expansion of $\vec{V}$ on the laser strength parameter a_0 up to the first order. The ρ_i parameters reduce to

$$\rho_0 \simeq \frac{1}{h_0^2} \left[h_0^2 - (1 + \cos \theta) h_0 v_z \right.$$

$$\left. - \, h_0 \sin \theta (v_x \cos \phi + v_y \sin \phi) \right],$$

$$\rho_1 = a_0 \frac{1}{h_0^2} [h_0 \sin \theta \sin \phi - v_y (1 + \cos \theta)], \qquad (35)$$

$$\rho_2 \simeq 0$$

and, by using the following small-argument expansion of the Bessel functions $J_p(x) = \delta_{0,p} + 1/2 \, x(\delta_{1,\,p} - \delta_{-1,\,p}) + \mathcal{O}(x^2)$, we can approximate $J_p(\rho_1 \omega / \omega_0)$ and $J_q(\rho_2 \omega / \omega_0)$ as

$$J_p(\rho_1 \omega / \omega_0) \simeq \delta_{0,\,p} + \frac{1}{2} \rho_1 \frac{\omega}{\omega_0} (\delta_{1,\,p} - \delta_{-1,\,p}),$$

$$J_q(\rho_2 \omega / \omega_0) \simeq J_q(0) = \delta_{0,\,q}. \qquad (36)$$

The resulting scattered-photon distribution is computed by Eq. (17) with

$$V_\theta \simeq -\frac{a_0}{h_0} \, \mathrm{sinc} \left(\Delta \omega_1 \frac{T}{2} \right) \left\{ \frac{1}{2h_0^2} \frac{\omega}{\omega_0} [\cos \theta \cos \phi v_x \right.$$

$$+ \cos \theta \sin \phi v_y - 2 \sin \theta h_0 v_z]$$

$$\times [h_0 \sin \theta \sin \phi - v_y (1 + \cos \theta)]$$

$$\left. + \left[\cos \theta \sin \phi + \sin \theta \frac{v_y}{4h_0} \right] \right\},$$

$$V_\phi = \frac{a_0}{h_0} \, \mathrm{sinc} \left(\Delta \omega_1 \frac{T}{2} \right) \left\{ \frac{1}{2h_0^2} \frac{\omega}{\omega_0} [\sin \phi v_x - \cos \phi v_y] \right.$$

$$\left. \times [h_0 \sin \theta \sin \phi - v_y (1 + \cos \theta)] - \frac{1}{2} \cos \phi \right\}. \qquad (37)$$

As expected, only the fundamental harmonic $\omega \approx \omega_F = \omega_0 / \rho_0$ is present.

To deal with a more tractable expression for the Thomson backscattering of a laser pulse with an ultra-relativistic electron having a small incidence angle $\theta_e \ll 1$, we employ the

small-angle approximation in Eq. (37), giving

$$\frac{d^2 N}{d\Omega d\omega} \simeq \frac{\alpha}{16(2\pi)^2} \frac{a_0^2 T^2}{\gamma_0^2} \left[1 - 4 \frac{(\gamma_0 \theta \sin \phi - \gamma_0 \theta_e \sin \phi_e)^2}{(1 + (\gamma_0 \tilde{\theta})^2)^2} \right]$$

$$\times \omega \, \mathrm{sinc}^2 \left(\frac{T}{2} (\rho_0 \omega - \omega_0) \right), \qquad (38)$$

where the ρ_0 parameter has been simplified as $\rho_0 \simeq (1 + (\gamma_0 \tilde{\theta})^2)/(4\gamma_0^2)$. We observe that the fundamental frequency $\omega_F = 4\gamma_0^2 \omega_0 / (1 + (\gamma_0 \tilde{\theta})^2)$ reduces to the well-known scattered-radiation frequency $4\gamma_0^2 \omega_0 / (1 + (\gamma_0 \theta)^2)$ for the case of backscattering onto an electron moving *on axis* (see e.g. [8]).

A further simplification (SALP) is obtained supposing both small angles and a very long pulse. In this case the spectral distribution of the photons emitted in a given direction is well approximated by a Dirac δ function, giving

$$\frac{d^2 N}{d\Omega d\omega}^{\mathrm{SALP}} \simeq \alpha N_c a_0^2 \frac{\gamma_0^2}{(1 + (\gamma_0 \tilde{\theta})^2)^2}$$

$$\times \left[1 - 4 \frac{(\gamma_0 \theta \sin \phi - \gamma_0 \theta_e \sin \phi_e)^2}{(1 + (\gamma_0 \tilde{\theta})^2)^2} \right]$$

$$\times \delta \left(\omega - \frac{4\gamma_0^2}{(1 + (\gamma_0 \tilde{\theta})^2)} \omega_0 \right). \qquad (39)$$

An integration over the photon energies is now straightforward and the resulting angular distribution can be expressed involving the differential cross section for the linear Thomson-scattering process $d\sigma/d\Omega$:

$$\frac{d\sigma}{d\Omega} \simeq 4r_0^2 \frac{\gamma_0^2}{(1 + (\gamma_0 \tilde{\theta})^2)^2}$$

$$\times \left[1 - 4 \frac{(\gamma_0 \theta \sin \phi - \gamma_0 \theta_e \sin \phi_e)^2}{(1 + (\gamma_0 \tilde{\theta})^2)^2} \right], \qquad (40)$$

where $r_0 = e^2 / m_e c^2$ is the classical electron radius and the angular integration of Eq. (40) yields the total Thomson cross section $\sigma_{\mathrm{Th}} = 8\pi r_0^2/3$. It is customary to note that the Thomson differential cross section (40) for electrons moving *on axis* in the pulse plateau ($v_\perp = 0$) reduces to the well-known cross section of the Thomson scattering valid for $\theta \ll 1$ and $\gamma_0 \gg 1$ (see e.g. [30]):

$$\frac{d\sigma}{d\Omega} \simeq 4r_0^2 \gamma_0^2 \frac{(1 + \gamma_0^4 \theta^4)}{(1 + \gamma_0^2 \theta^2)^4}. \qquad (41)$$

We conclude this subsection by giving an approximated expression for the spectral distribution $S(\omega) = dN/d\omega$ in the SALP limit of the scattered photons which are generated by linear Thomson backscattering of an electron moving *on axis* in the pulse plateau and collected forward of the electron velocity within a cone of half-aperture θ_{Max}. This expression can be employed to obtain a rough expression for the spectral distribution of the radiation generated with very low transverse emittance electron bunches (see Sect. 3) and it is simply obtained from Eq. (39) with a straightforward change

in variables, giving

$$
S(\omega) = \begin{cases}
\dfrac{\alpha}{64}\dfrac{T a_0^2}{\omega_0^2 \gamma^6}\left(\omega^2 - 4\omega\omega_0\gamma^2 + 8\omega_0^2\gamma^2\right) \\
\text{if}\quad \dfrac{4\gamma^2\omega_0}{1+\gamma^2\theta_{\text{Max}}^2} \le \omega \le 4\gamma^2\omega_0, \\
0, \quad \text{otherwise.}
\end{cases}
\tag{42}
$$

2.8 *Radial inhomogeneity effects*

We are now able to deduce *a posteriori* simple relations stating the strength of the effects produced by the radial dependence of the laser pulse amplitude on the scattered-radiation distribution. A 'direct' effect is merely induced by the dependence of the peak frequency and angular distribution of the harmonics on the square of the laser strength ($a(r) = a_0 \exp(-r^2/w_0^2)$ for a standard Gaussian profile), which in turn introduces a dependence of the scattered-radiation distribution on the radial distance r of the particle from the pulse axis. An 'indirect' effect is caused by the transverse ponderomotive forces, which generate a particle transverse momentum, thus inducing the particles to escape from the on-axis region of the pulse.

Let us consider an electron moving relativistically ($\gamma_0 \gg 1$) with a small angle θ_e (i.e. $v_\perp \ll v_z \simeq \gamma_0$) and experiencing a head-on collision with a pulse. As has been stated in Sect. 2, if the pulse has a large amplitude the *longitudinal ponderomotive forces* of the rising front do reduce the longitudinal momentum of the electron during the interaction $\bar{u}_z$, which is lower than its initial momentum by a factor $\bar{u}_z/u_{z0} \simeq 1 - a_0^2/8\gamma_0^2$ (see Eq. (10)), so that the incidence angle of the interacting particle is amplified correspondingly:

$$
\tan\bar{\theta} \simeq \frac{\theta_e}{1 - a_0^2/8\gamma_0^2}.
\tag{43}
$$

Note that $\tan\bar{\theta}$ diverges if a_0 approaches $\sqrt{8}\gamma_0$, so in the following we will consider only scenarios in which $\tan\bar{\theta} \simeq \bar{\theta}$, i.e. the incidence angle of the particle inside the pulse is well below unity. The particle interacts with the pulse for a time $t_{\text{int}} = T/(1+\beta_z^L) \simeq T(1+a_0^2/8\gamma_0^2)/2$, which has its minimum value of $T/2$ for a low-intensity pulse ($a_0 \ll \sqrt{8}\gamma_0$).

We consider first the direct geometric effects. The radial coordinate of the particle during its interaction with the pulse varies in the range $[r_0 - \bar{\theta}(ct_{\text{int}}), r_0 + \bar{\theta}(ct_{\text{int}})]$ and should be compared with the pulse waist w_0. Therefore, an effective radial coordinate $r_{\text{eff}} \equiv \sqrt{r_0^2 + (\bar{\theta}ct_{\text{int}})^2}$ can be introduced. As a result, geometric radial inhomogeneity effects are negligible if the initial radial position and incidence angle of the electron satisfy

$$
r_{\text{eff}}^2 = r_0^2 + \left(\frac{\theta_e cT}{2\beta_z^L}\right)^2 < w_0^2,
\tag{44}
$$

where $\beta_z^L \simeq (1 - a_0^2/8\gamma_0^2)/(1 + a_0^2/8\gamma_0^2)$ (see Sect. 2).

A second effect is the radial drift velocity produced by transverse ponderomotive forces (TPF), which have been fully neglected in the derivation of the particle trajectories. Let us

now switch on TPF (see e.g. [34] and references therein) in the particle dynamics:

$$
F_p^\perp = -\frac{e^2}{2m_e\bar{\gamma}c^2}\nabla_\perp(|A|^2),
\tag{45}
$$

where $\bar{\gamma}$ is a mean over a pulse oscillation of $\gamma = (1 + \vec{u}^2(t))^{1/2}$. The time derivative of the normalized transverse momentum can then be written in terms of the transverse spatial derivative of the normalized pulse amplitude as

$$
\left(\frac{du_\perp}{dt}\right)_{\text{TPF}} \simeq \frac{c}{2\bar{\gamma}}\nabla_\perp a^2.
\tag{46}
$$

With the hypothesis that TPF will introduce small changes in the particle dynamics and by using relations (6) with $(|v_x|, |v_y|) \ll v_z \simeq \gamma_0$, we find $\bar{\gamma} \simeq \gamma_0(1 + a_0^2/8\gamma_0^2)$, so that the variation induced by TPF of the radial momentum can be estimated as

$$
\delta u_\perp^{\text{TPF}} \gtrsim \left(\frac{du_\perp}{dt}\right)_{\text{TPF}} t_{\text{int}} \simeq \left(\frac{(cT)r_{\text{eff}}a_0^2}{\gamma_0 w_0^2}\right).
\tag{47}
$$

Equation (47) is valid provided that $|\delta u_\perp^{\text{TPF}}| \ll \sqrt{(\bar{u}_\perp)^2} \simeq a_0/\sqrt{2}$, so that the relation $(cT)r_{\text{eff}}a_0/\gamma_0 w_0^2 \ll 1$ must be fulfilled, too.

The net effect of the transverse ponderomotive forces is the refraction of the particles away from the pulse axis, with a refraction angle $\theta_R \simeq \delta u_\perp^{\text{TPF}}/\bar{u}_z \simeq (cT)r_{\text{eff}}a_0^2/[\gamma_0^2 w_0^2(1 - a_0^2/8\gamma_0^2)]$. A criterion for determining the validity of neglecting transverse ponderomotive forces in the estimation of the Thomson-scattered radiation is obtained by imposing an upper limit on θ_R. As before, the radial excursion of the particle during the interaction with the pulse should not exceed the pulse waist, which means that $\theta_R < 2w_0/[cT(1 + a_0^2/8\gamma_0^2)]$ or

$$
\frac{a_0^2(cT)^2 r_{\text{eff}}}{2\gamma_0^2 \beta_z^L w_0^3} < 1
\tag{48}
$$

must hold true. Note that Eq. (48) can be rewritten by defining an effective *incidence angle*

$$
\theta_{\text{TPF}} \equiv (cT)r_{\text{eff}}a_0^2/(\gamma_0^2 w_0^2),
\tag{49}
$$

which takes into account the effects of TPF since the very beginning, and imposing that (see Eq. (44))

$$
\theta_{\text{TPF}} < 2\beta_z^L w_0/cT.
\tag{50}
$$

As a result, the effect of TPF is to increase the incidence angle of the particle to a value $\theta_{\text{eff}} \approx \sqrt{\theta_e^2 + \theta_{\text{TPF}}^2}$, so that θ_{TPF} should be taken into account when we make estimations of the blurring effects on the scattered-photon spectrum.

If relations 44 and 50 are fulfilled, the relative shift of the fundamental frequency of the radiation emitted by two particles having ($r_0 \neq 0$, $v_\perp \neq 0$) and ($r_0 = 0$, $v_\perp = 0$), respectively, can be approximately estimated as

$$
\delta\omega_F/\omega_F \simeq \frac{\delta(a_0^2/2)}{(1 + \gamma_0^2\tilde{\theta}^2 + a_0^2/2)}
$$

$$
\simeq \frac{2a_0^2}{(1 + \gamma_0^2\tilde{\theta}^2 + a_0^2/2)}\left(\frac{r_{\text{eff}}^2 + (\theta_R ct_{\text{int}})^2}{w_0^2}\right).
\tag{51}
$$

The blurring in the scattered-radiation distribution introduced by the radial dependence of the pulse amplitude is then *of the second order* in the ratios $\theta_R(ct_{int})/w_0$ and r_{eff}/w_0 and it is more evident when the photons are collected *forward* of the initial direction of motion of the particle.

3   Thomson backscattering by an electron bunch

In dealing with the estimation of the scattered-photon distribution generated by the head-on collision of an electron bunch and a laser pulse, we have to sum up *incoherently* the contributions of the single electrons, i.e. we integrate over the scattered-photon distributions of the particles of the bunch. The computation of $d^2N/d\omega d\Omega$ reported here is valid provided that the pulse is linearly polarized (along y, for instance) and flat topped. The employed plane-wave approximation also imposes a higher limit for the bunch (σ_L) and pulse (cT) lengths, namely ($\sigma_L, cT(1 + a_0^2/8\gamma_m^2)/2) \ll Z_R = \pi w_0^2/\lambda_0$, where γ_m is the minimum Lorentz factor of the particles in the bunch. Also, for a given pulse duration, the charge of the bunch should be low enough to let the space-charge effects be negligible during the interaction [7]. In order to neglect the pulse transverse inhomogeneity effects, the transverse bunch size σ_T should be smaller than the pulse waist *and* the angular divergence $\Delta\theta_e$ of the bunch should satisfy the relations (44) and (50) with the substitutions $r_0 \rightarrow \sigma_T$, $\theta_e \rightarrow \Delta\theta_e/2$ and $\gamma_0 \rightarrow \gamma_m$. Moreover, for extremely short pulses, we must take into account the effect of the pulse rising front, too. Since in the plateau the temporal mean of the transverse momentum along y is $v_y \equiv \bar{u}_y = u_{y0} + \bar{a}$, it is mandatory that the initial phase ϕ_0 be fine tuned so as to ensure that $\bar{u}_y/\bar{u}_z < \Delta\theta_e$.

By introducing the transverse $\Theta(\gamma, \theta_e, \phi_e, r_e)$ and spectral $F(\gamma)$ distributions of the electrons having initial energy $E = \gamma m_e c^2$, incidence angles (θ_e, ϕ_e) and radial coordinate r_e we can write the total scattered-photon distribution of an electron bunch as

$$\frac{d^2N}{d\Omega d\omega}\Big|_{Bunch} = \sum_i \left(\frac{d^2N}{d\Omega d\omega}\right)_{i\text{th electron}}$$

$$= \int d\gamma d\theta_e d\phi_e dr_e F(\gamma)\Theta(\gamma, \theta_e, \phi_e, r_e)$$

$$\times \left(\frac{d^2N}{d\Omega d\omega}\right)_{\gamma, \theta_e, \phi_e, r_e}, \quad (52)$$

where $(d^2N/d\Omega d\omega)_{\gamma, \theta_e, \phi_e, r_e}$ is the photon distribution produced by an electron with energy $\gamma m_e c^2$, incidence angles (θ_e, ϕ_e) and initial radial coordinate r_e.

Expression (52) can be applied both in the exact relation (18) and in all the simplified limiting cases described in the previous section and it shows the simplest form in the case of linear Thomson scattering in the SALP limit:

$$\frac{d^2N}{d\Omega d\omega}\Big|_{Bunch}^{SALP} \simeq \alpha N_c a_0^2 \int d\gamma d\theta_e d\phi_e dr_e \exp\left(-2r_e^2/w_0^2\right)$$

$$\times F(\gamma)\Theta(\gamma, \theta_e, \phi_e, r_e)\frac{\gamma^2}{(1 + (\gamma\tilde{\theta})^2)^2}$$

$$\times \left[1 - 4\frac{(\gamma\theta\sin\phi - \gamma\theta_e\sin\phi_e)^2}{(1 + (\gamma\tilde{\theta})^2)^2}\right]$$

$$\times \delta\left(\omega - \frac{4\gamma^2}{(1 + (\gamma\tilde{\theta})^2)}\omega_0\right), \quad (53)$$

where $\tilde{\theta}^2 = \theta^2 + \theta_e^2 - 2\theta\theta_e\cos(\phi - \phi_e)$.

A remark is needed here. In a previous work of Catravas et al. [8] (see also [14]), a relation linking the scattered-radiation distribution for an electron bunch to the yield of a single electron moving *on axis* was given in the case of small scattering and incidence angles and nonrelativistic quivering. The relation involved a convolution in the form

$$\frac{d^2N}{d\Omega d\omega}(\omega, \theta, \phi)$$

$$\simeq \int d\gamma \int d\theta_e dr_e \exp\left(-2r_e^2/w_0^2\right)$$

$$\times F(\gamma)\Theta(\gamma, \theta_e, r_e)\left(\frac{d^2N}{d\Omega d\omega}\right)_\gamma^{\theta_e=0}(\omega, \theta - \theta_e, \phi), \quad (54)$$

where invariance over the azimuthal angle of the particle distribution was supposed and where $(d^2N/d\Omega d\omega)^{\theta_e=0}$ means the scattered-photons distribution generated by a single electron having $\theta_e = 0$. The relations (53) and (54) *do not* match. However, Eq. (54) is an approximation of Eq. (53) obtained by substituting ϕ_e with ϕ (case $\theta_e \geq 0$) or $\phi - \pi$ (case $\theta_e < 0$), by which $\tilde{\theta} \rightarrow (\theta \mp \theta_e)$ for $\theta_e \geq 0$. We stress that, as will clear below, Eq. (54) is a good approximation of (53) in the case $\theta \ll \theta_e$ but it underestimates the effects of the bunch divergence when $\theta \gtrsim \theta_e$.

To apply the linear Thomson scattering formula (53), we consider first the simplest case of backscattering between a pulse having $a_0 \ll 1$ and a bunch with a negligible angular divergence, Gaussian transverse spatial envelope $\Phi(r_e) = r_e \exp(-r_e^2/2\sigma_T^2)/(2\pi\sigma_T^2)$ and a small energy spread $\Delta E_{FWHM}/E \ll 1$. Since the incidence angle θ_e of each particle is null, we immediately note that, once the acceptance angle θ_{Max} is fixed, the spectral distribution of the collected photons can be obtained analytically from Eq. (42) by taking also into account the dependence of the pulse amplitude on the radial coordinate. This can be pursued by introducing a *filling factor*

$$\mathcal{F} \equiv \left[\int dr_e \exp\left(-2r^2/w_0^2\right)\Phi(r_e)\right]\Big/\left[\int dr_e \Phi(r_e)\right]$$

which in this case reduces to $\mathcal{F} = (w_0^2/[w_0^2 + 4\sigma_T^2])$. A complete computation of the spectrum would require that an energy integration over the particle's energy is performed. However, for the case of bunches with small energy spread, the particle's energy distribution can be approximated as a Dirac delta function, obtaining a scattered radiation spectrum of the form

$$S(\omega) = (\mathcal{F}N_e)\begin{cases} \dfrac{\alpha}{64}\dfrac{Ta_0^2}{\omega_0^2\gamma^6}(\omega^2 - 4\omega\omega_0\gamma^2 + 8\omega_0^2\gamma^2) \\ \text{if} \quad \dfrac{4\gamma^2\omega_0}{1 + \gamma^2\theta_{Max}^2} \leq \omega \leq 4\gamma^2\omega_0, \\ 0, \quad \text{otherwise,} \end{cases} \quad (55)$$
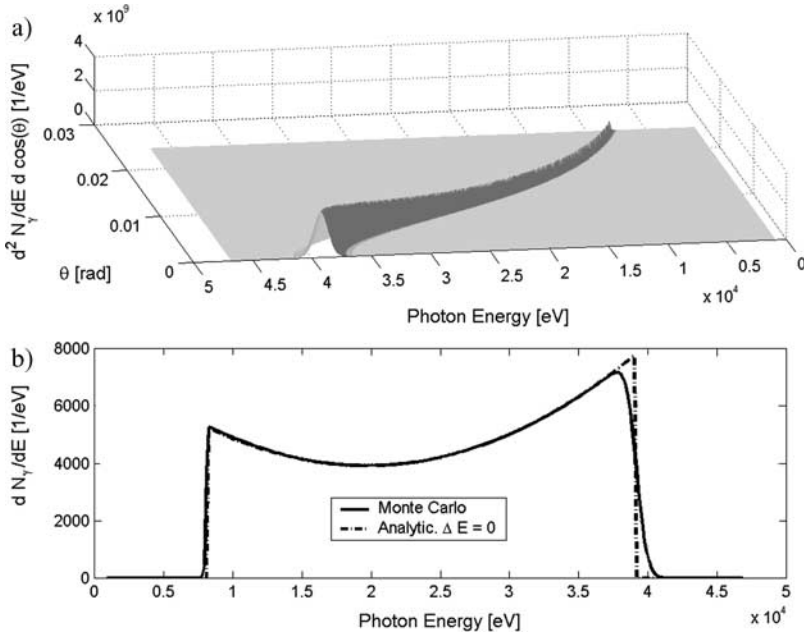
FIGURE 6 **a** Angular and spectral distribution integrated over the azimuthal angle of the scattered photons of a Ti:Sa laser pulse of flat-top temporal profile with duration $T = 1$ ps, peak amplitude $a_0 = 0.1$ and waist size $w_0 = 30$ μm and an electron bunch with negligible angular divergence and narrow energy distribution with mean energy of 40 MeV ($\gamma = 80$) and spread $\delta E/E = 2.5\%$. The distribution has been obtained by summing up the contributions of randomly generated sample particles. **b** Spectral distribution of the radiation collected within a cone of half-aperture $\theta_{Max} = 2/\gamma = 250$ mrad. The *solid line* has been obtained by integrating the distribution in (**a**) and the *dashed line* is the analytical result (55) valid for both negligible divergence and energy spreads

γ being the mean Lorentz factor of the bunch. This formula is very useful when we want to get started with the estimations of the expected spectral width and the number of photons, provided that the acceptance angle is fixed. As a first result, we note that the nonzero part of $S(\omega)$ is almost flat, so that the energy spread is basically given by the maximum and minimum energies in the range, i.e. $\delta\omega/\max(\omega) \simeq \gamma^2\theta_{Max}^2$, thus giving a spread of 100% for $\theta_{Max} = 1/\gamma$. Let us introduce the parameter $\psi = \theta_{Max}\gamma$ and let $N_{Acc}(\psi)$ be the number of photons collected into a cone of half-aperture $\theta_{Max} = \psi/\gamma$. In the limit of very small energy spread and angular divergence of the bunch, N_{Acc} can be estimated by integrating Eq. (55), giving

$$N_{Acc}(\psi) = (\mathcal{F}N_e)\frac{1}{2}\alpha\omega_0 T a_0^2 \psi^2 \frac{(1 + \psi^2 + 2\psi^4/3)}{(1 + \psi^2)^3}. \quad (56)$$

Note that for $\psi \ll 1$, $N_{Acc} \propto \psi^2$ and $\delta\omega/\omega \simeq \psi^2$, so that the well-known relation $N_{Acc} \propto (\delta\omega/\omega)$ is recovered (see e.g. [8]). We compare the spectrum (55) with that obtained by summing up the contributions of a set of 10^3 randomly generated sample particles (Monte Carlo estimation) of a bunch having mean energy $E = 40$ MeV, energy spread $\Delta E_{FWHM}/E = 2.5\%$ and transverse size $\sigma_T = 10$ μm, colliding with a pulse with a waist size $w_0 = 30$ μm and duration $T = 1$ ps. The scattered-photon distribution of each sample particle has been obtained with the SALP formula for the linear Thomson scattering (38). The results for an acceptance angle $\theta_{Max} = 2/\gamma = 250$ mrad ($\psi = 2$), reported in Fig. 6, clearly show the accuracy of the simple estimation (55).

Equation (56) states that the efficiency of the linear Thomson scattering process increases with the bandwidth of the collected radiation. This means that, among the possible applications of such X-ray sources, those employing X-rays with moderately low energy spread can take advantage of the larger number of photons irradiating target. Mammography [35] is a pertinent example of such an application, since it can employ Thomson-scattered X-ray

beams with an energy spread of the order of 20% without a sizable reduction of image quality with respect to the images obtained with monochromatic synchrotron-radiation sources [S. Stumbo, U. Bottigli, B. Golosio and P. Oliva, *private communication* (2004)]. If, instead, the aim is to produce quasi-monochromatic X-rays, the radiation must be collected into a cone of very small aperture, i.e. small ψ's are required. To show this, we report in Fig. 8a) a sequence of spectra obtained with the Monte Carlo method by using progressively smaller acceptance angles, as well as the analytic result (55) with $\psi = 0.3$. In Fig. 8b) we show the number of collected photons as a function of ψ for both the analytical and Monte Carlo estimations, which seem to agree remarkably well.

Consider now the linear Thomson scattering process of a laser pulse and a bunch presenting negligible energy spread but sizable angular divergence. We focus on a bunch having energy $E_b = 40$ MeV and divergence $\Delta\theta_e = 25$ mrad, by computing the spectrum of the scattered photons collected within three acceptance angles ($\theta_{Max} = 12$ mrad, 25 mrad and 65 mrad). The comparison between the spectra obtained with Eqs. (53) and (54) (see Fig. 7) clearly confirms a good agreement between the two curves for $\theta_{Max} \ll \theta_e$, while the simplified expression 54 completely fails in estimating the spectral distribution for $\theta_{Max} \gg \theta_e$.

The formulas derived in Sect. 2 for the Thomson backscattering of a laser pulse moving exactly along the z axis by a quasi-counterpropagating electron constitute useful tools to evaluate (e.g. via Monte Carlo methods) the distribution of the photons scattered by an ultra-relativistic electron bunch with reasonably good beam quality. If Thomson backscattering is employed with the aim to generate short, quasi-monochromatic and bright X-ray pulses (Laser Synchrotron Source, LSS), the key bunch parameters are the beam energy, charge and emittance. The charge and mean energy control the total number of scattered photons and their maximum energy, while
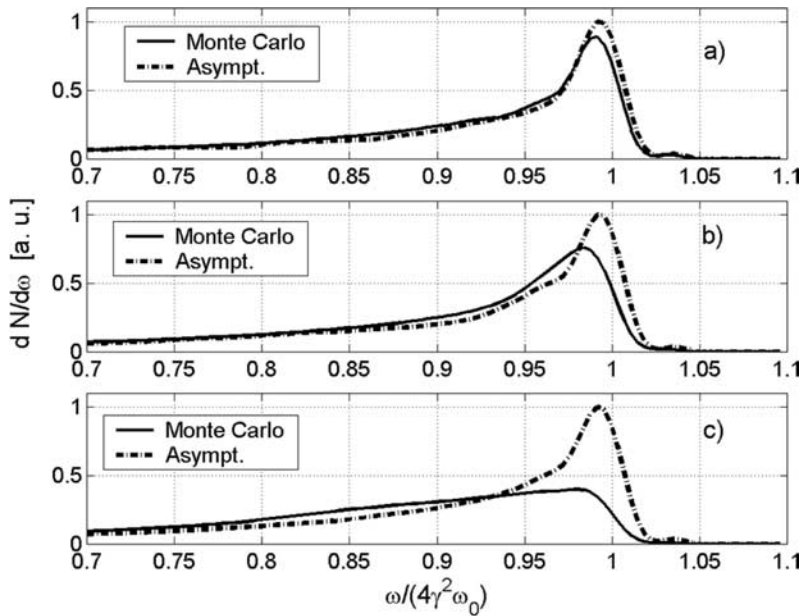
FIGURE 7 Spectral distribution of the photons produced by linear Thomson scattering between a pulse with $N_c \gg 1$ and an electron bunch of mean energy $E_b = 40$ MeV presenting a negligible energy spread but sizable angular divergence $\Delta\theta_e = 25$ mrad. Both the Monte Carlo computation based on Eq. (42) and the simplified expression used in the literature (Eq. (54)) are employed. **a** Results for an acceptance angle $\theta_{Max} = 12$ mrad. The simplified computation agrees quite well with the detailed estimation. **b** Results for an acceptance angle $\theta_{Max} = 25$ mrad. The matching between the two curves is not very good. However, the simplified expression still gives a reasonable spectrum. **c** Results for an acceptance angle $\theta_{Max} = 65$ mrad. The matching between the two curves is now very poor

the emittance basically limits the possibility to reduce the energy spread of the collected photons. On the laser pulse side, the product between the wavelength and the delivered energy is proportional to the number of incoming (and thus to the scattered) photons. Here, we will concentrate on the effect of the bunch divergence, since many details of LSS have been reported elsewhere (see e.g. [7–9]).

In the following we will consider two kind of bunches. The first is produced by standard RF photocathode guns, which can generate beams with a remarkably good quality (see e.g. [36]). The second kind is obtained by using laser–plasma accelerators with some controlling technique of the beam-injection mechanism [37–40], which seems to be able (at least in 'virtual experiments') to produce electron bunches with low emittances as well.

3.1 *Standard RF guns*

3.1.1 Linear regime. We now analyze the case of an X-ray source of photons having energy $E_X \simeq 40$ keV, a typical value for X-rays employed for medical diagnostics [23, 24]. We consider a laser pulse of wavelength $\lambda_0 = 0.8\,\mu$m ($E_0 = 1.56$ eV) and an electron bunch of energy $E_b = 40$ MeV, charge $Q_b = 1.6$ nC, transverse size $\sigma_T = 10\,\mu$m and length $\sigma_L = 150\,\mu$m. Such a bunch thus contains $N_e = 10^{10}$ electrons moving with $\gamma_0 \approx 80$ roughly along the z axis and experiencing a head-on collision with the pulse. The laser system delivers pulses of energy $E_L = 0.4$ J and duration $T = 1$ ps with a flat-top temporal profile, with a Gaussian transverse envelope of waist $w_0 = 30\,\mu$m. Since for such a long pulse duration the pulse rise time can be of the order of a hundred femtoseconds, we assume that the mean potential $\bar{a}$ is
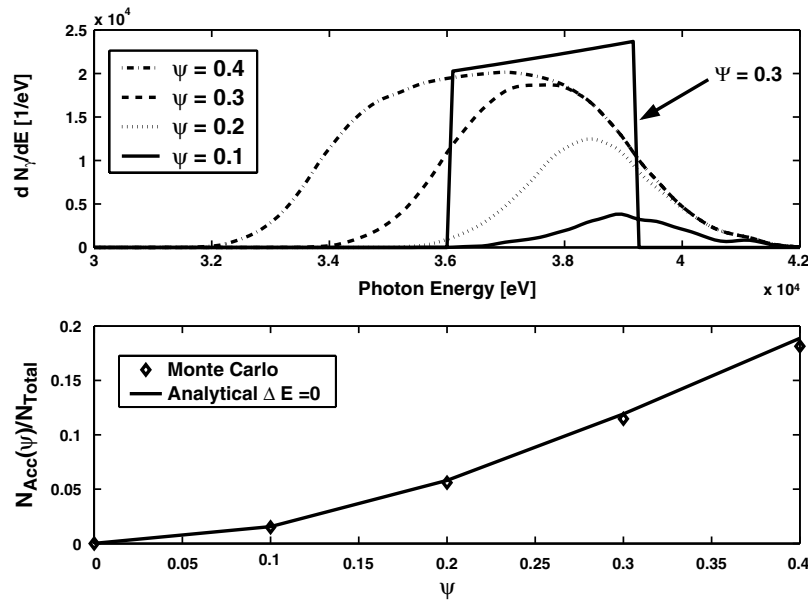

FIGURE 8 a Spectral distributions of the scattered photons for a system as in Fig. 6, obtained with different acceptance angles $\theta_{Max} = \psi/\gamma$. The *thick solid line* has been obtained with the analytic spectrum (55) for $\psi = 0.3$. **b** Total number of collected photons $N_{Acc}(\psi)$ for both the Monte Carlo and analytic estimations. The numbers have been normalized to the total scattered photon number $N_{Total} = 2N_{Acc}(\psi = 1)$
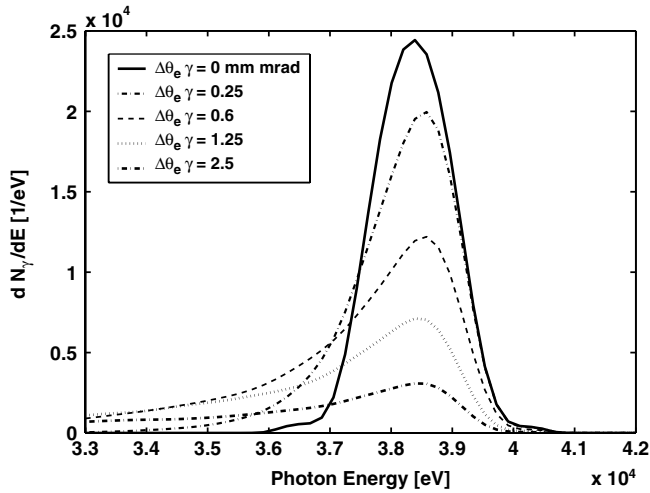
FIGURE 9 Spectral distributions of the scattered photons in a scattering process by a pulse having the same characteristics as in Fig. 6. The bunches have now a narrow energy distribution with $\Delta E/E = 0.25\%$ and a Gaussian distribution in the incidence angle θ_e with variance $\sigma_\theta = \Delta\theta_e/\sqrt{8\log 2} \simeq \Delta\theta_e/2.35$. The spectra of the scattered photons are obtained by integrating the spectral and angular distributions within an acceptance angle $\theta_{Max} = 0.2/\gamma$. Several bunches with different emittances and thus divergences $\Delta\theta_e \simeq 2\epsilon_n^\perp/\gamma\sigma_T$ up to $\Delta\theta_e \simeq 2/\gamma$ are considered

completely negligible. Both the bunch ($\sigma_L = 150\,\mu m$) and the pulse ($cT \simeq 300\,\mu m$) lengths are much lower than the Rayleigh length $Z_R = \pi w_0^2/\lambda_0 \simeq 3500\,\mu m$, so that the plane-wave approximation holds. Also, since the peak amplitude is $a_0 = 0.1 \ll 1$, linear Thomson-scattering formulas will be used.

Our calculations are valid provided that the bunch angular divergence is limited to $\Delta\theta_e \gtrsim 2w_0/cT \approx 200\,mrad$, a very large value if compared to record numbers of a few milliradians of modern RF photoguns. Because of the low value of a_0, transverse ponderomotive forces can also be neglected. The scattered-photon distribution is obtained with a Monte Carlo method by summing up the contributions of single particles in the SALP limit (see Eq. (53)).

In the following, we will consider several bunches presenting different values of transverse normalized emittances $\epsilon_n^\perp \simeq \gamma\sigma_T\Delta\theta_e/2$. As in the case of negligible angular divergence, we will be mainly interested in the spectral distribution of the scattered radiation, which will be estimated with a Monte Carlo method based on the SALP approximation (Eq. (53)). The randomly generated sample particles are now distributed with a very narrow energy spread (namely $\Delta E_b/E_b = 0.25\%$, a value reachable with currently available RF photoguns). Such a spread introduces a very small energy spread $\delta\omega/\omega \simeq 2\Delta E_b/E_b \simeq 0.5\%$ on the scattered radiation, so that the angular divergence effects can be clearly highlighted. In Fig. 9 the spectra of the scattered radiation collected into a cone of half-aperture $\theta_{Max} = 0.2/\gamma$ for beam transverse normalized emittances ranging from 0 to 10 mm mrad are reported. For a transverse size of the beam $\sigma_T = 10\,\mu m$ the beams are characterized by angular divergences reaching $\Delta\theta_e\gamma \simeq 2$. The net effect of the angular divergence is, as is well known, a spreading of the energy distribution of the scattered photons. To reach the goal of a 5% FWHM energy spread, for example, a bunch with angular divergence not exceeding $\Delta\theta_e = 0.6/\gamma$ ($\sigma_e \lesssim 0.25/\gamma$), i.e. having $\epsilon_n^\perp \lesssim 2.5\,mm\,mrad$ with $\gamma = 80$ and $\sigma_T = 10\,\mu m$, should be employed.

We stress that our detailed estimation differs substantially from that of the simplified expression (54). In Fig. 10a, in fact, the spectra obtained with the two methods of the radiation for a collecting angle $\theta_{Max} = 0.2/\gamma$, for both the cases $\Delta\theta_e = 0.25/\gamma$ and $\Delta\theta_e = 0.6/\gamma$, do not match. In particular, both the peak frequency and the energy spread do differ in a sizable way, with a clear underestimation of the beam-divergence effects when the simplified expression (54) is employed.

In Fig. 10b the relative number of collected photons $N_{Acc}(\Delta\theta_e)/N_{Acc}(\Delta\theta_e = 0)$ as a function of the beam divergence is reported. The circle and diamond points represent the data obtained with the detailed formula (53) and the simplified expression (54), respectively, while the solid line shows a fit of the detailed data with the function $N_{Acc}(\Delta\theta_e)/N_{Acc}(\Delta\theta_e =$
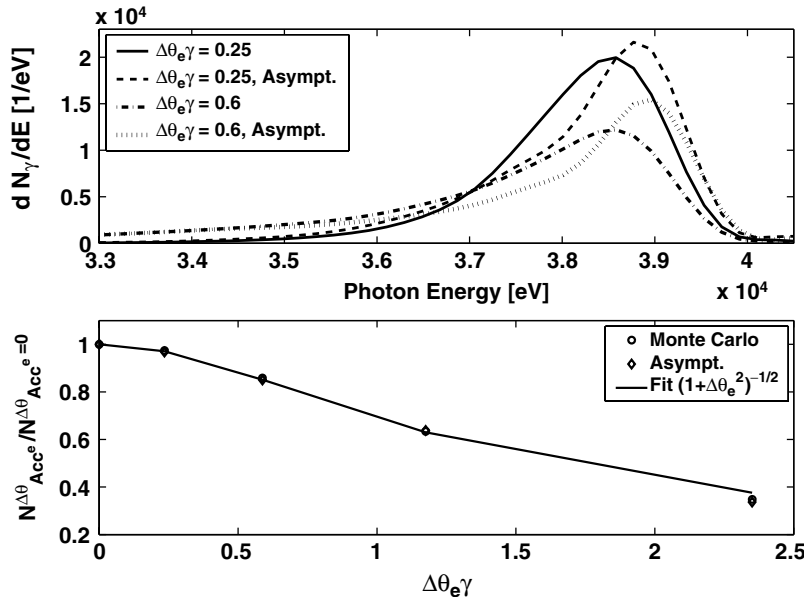

FIGURE 10 Spectral distributions of the scattered photons for systems as in Fig. 9. **a** Comparison between the spectra estimated with the SALP formula and the simplified expression (54) for the case of angular divergence $\Delta\theta_e\gamma = 0.25$ (*solid line* and *dashed line*, respectively) and for the case $\Delta\theta_e\gamma = 1.25$ (*dash-dotted line* and *dotted line*, respectively). **b** Number of collected photons normalized to the case of null beam divergence versus beam divergence and fit of the data with a function $1/\sqrt{1+\Delta\theta_e^2}$ (*solid line*)

$0) = 1/\sqrt{1 + \Delta\theta_e^2}$. We note that in this case the simplified expression (54) gives results that are in good agreement with the ones obtained with the more sophisticated estimation (53).

3.1.2 Nonlinear regime. To switch in the nonlinear regime, we consider three cases of Thomson backscattering of pulses having the same duration of $T = 30$ fs but different energies, namely $E_L^{(1)} = 0.5$ J, $E_L^{(2)} = 5$ J and $E_L^{(3)} = 50$ J, at the wavelength of 832 nm. In order to suppress transverse effects, we consider pulses having a waist size of $w_0 = 50$ μm, a bit larger than the previous case. Moreover, we will suppose that a pulse-shaping technique, producing pulses with flat-top longitudinal profiles with rise time $T_R = 6$ fs, is employed. The normalized pulse amplitudes with the parameters sketched above are $a_0^{(1)} = 0.32$ (almost linear regime), $a_0^{(2)} = 1$ (weakly nonlinear regime) and $a_0^{(3)} = 3.2$ (fully nonlinear regime). Since the rise time is small, the value of the mean potential should be estimated carefully. Supposing a shape $H(\xi) = \sin^2(\pi\xi/2T_R)$ for $0 \leq \xi \leq T_R$, we found that $\bar{a}$ oscillates with the initial phase ϕ_0 with an amplitude $\bar{a}_{max}/a_0 = 0.07$. This implies that $\bar{a}$ can reach the value of 0.22 for the fully nonlinear case.

The colliding electron beams have transverse emittance $\epsilon_n^\perp = 5$ mm mrad and they have been focused in a spot of transverse size $\sigma_T = 5$ μm. To keep the fundamental frequency ω_F the same as the linear case, the bunch energies are left to vary accordingly with the pulse amplitude a_0, as $E_b = 40\sqrt{1 + 1/2a_0^2}$ MeV, ranging from $\simeq 40$ MeV for the case (1) to $\simeq 100$ MeV for the case (3). Note that since the beams have a common value of the transverse emittance but different energies, they have different angular divergences $\Delta\theta_e \simeq 4\epsilon_n^\perp/(\sigma_T 40\sqrt{1 + 1/2a_0^2})$ too, ranging from 40 mrad for the case (3) to 100 mrad for the case (1). We stress also that the transverse momentum induced during the pulse rising front $-\bar{a}$ does not affect the particle dynamics, since it is associated with an effective incidence angle $\simeq 2\bar{a}/E_b$ reaching the value of 2.2 mrad (fully nonlinear case), a value which is well below the bunch divergence.

The beam and pulse parameters allow the radial inhomogeneity effects to be fully neglected. For the worst case (3), in fact, both the transverse beam size and the divergence satisfy Eq. (44) and transverse ponderomotive forces introduce an effective incidence angle of $\theta_{TPF} \simeq 10^{-3}$ mrad that is negligible with respect to the bunch divergence.

The Thomson backscattered photon distributions have been estimated by using the SALP approximation in the nonlinear regime and the resulting spectral and angular distributions integrated over the azimuthal angle ϕ, for both the pulses of minimum and maximum energies, are reported in Fig. 11.

In the nonlinear regime both incidence and scattering angles do have a minor effect on the scattered-photon distribution compared to the linear case, since their natural weight is now $\sqrt{1 + a_0^2/2}/\gamma$ rather than $1/\gamma$. The resulting reduction of the blurring effects caused by the angular divergence of the beam is evident by comparing Fig. 11a and b, where the first-harmonic yield is shown. This is clearer in Fig. 12, where the normalized spectra obtained by integrating the spectral and angular distributions up to an angle $\theta_{Max} = \psi\sqrt{1 + a_0^2/2}/\langle\gamma\rangle$ with $\psi = 0.2(\theta_{Max} \simeq 15$ mrad) are reported.

3.2 *Laser–plasma accelerator*

The idea of using laser–plasma-accelerated bunches to produce Thomson-scattered radiation was first analyzed in detail by Catravas et al., who considered bunches produced either with self-modulated laser wake-field accelerators (SM-LWFAs) or laser wake-field accelerators (LWFAs) with optically controlled trapping (see [8] and references therein). The estimations reported in Ref. [8], however, considered only the linear regime and are based on the simplified expression (54), which has been proved to be an approximation of Eq. (53). Recently, Hafz et al. [39] have performed a two-dimensional (2D) numerical simulation of laser–plasma interaction in the regime of laser wake-field acceleration with particle injection induced by the presence of a sharp
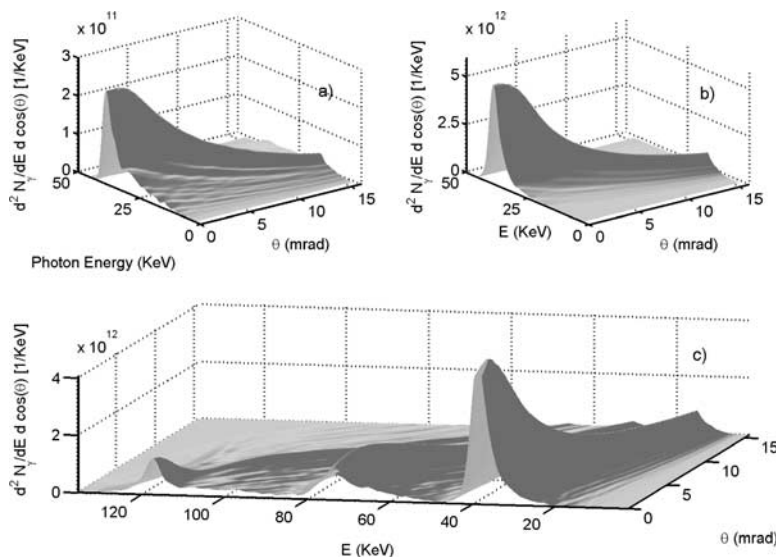

FIGURE 11 Spectral and angular distribution integrated over the azimuthal angle ϕ of the Thomson-backscattered photons produced by the collision between linearly polarized, flat-top pulses of duration $T = 30$ fs and rise time $T_R = 6$ fs, energies $E_L^{(1)} = 0.5$ J and $E_L^{(3)} = 50$ J, wavelength $\lambda_L = 0.832$ μm and focused in a spot of size $w_0 = 50$ μm. The normalized pulse amplitudes are $a_0^{(1)} = 0.32$ and $a_0^{(3)} = 3.2$, respectively. The employed electron bunches have energies $E_b^{(1)} = 40\sqrt{1 + a_0^2/2} \simeq 41$ MeV and $E_b^{(3)} = 40\sqrt{1 + a_0^2/2} \simeq$ 99 MeV, transverse emittance $\epsilon_n^\perp = 5$ mm mrad and transverse size $\sigma_T = 5$ μm. **a** Distribution for the linear case (1). **b** Distribution of the *first harmonic* for the fully nonlinear case (3). **c** Distribution of the first three harmonics for the case (3)
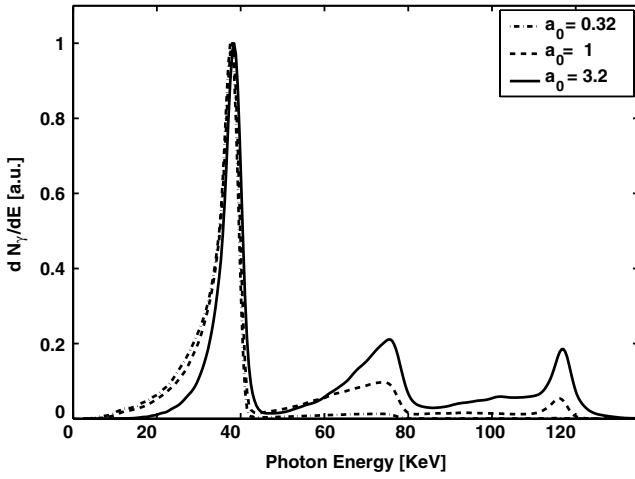
FIGURE 12   Normalized spectral distributions of the Thomson-scattered radiation produced by three laser and pulse parameters. The *dashed line* is obtained with a pulse as in Fig. 11 with energy $E_L^{(1)} = 0.5$ J ($a_0^{(1)} = 0.32$, linear regime) and a beam of mean energy $E_b^{(1)} = 40\sqrt{1 + a_0^2/2} \simeq 41$ MeV. The acceptance angle is $\theta_{Max}^{(1)} = \psi\sqrt{1 + a_0^2/2}/\langle\gamma\rangle$ with $\psi = 0.2$. The *dash-dotted line* is obtained with a pulse of energy $E_L^{(2)} = 5$ J ($a_0^{(2)} = 1$, weak nonlinear regime) and a beam of mean energy $E_b^{(2)} = 40\sqrt{1 + a_0^2/2} \simeq 50$ MeV. The *solid line* is obtained with the pulse and beam in the full nonlinear regime $E_L^{(3)} = 50$ J and a beam of mean energy $E_b^{(3)} = 40\sqrt{1 + a_0^2/2} \simeq 99$ MeV

plasma-density transition [38]. They applied the results in Ref. [7] to estimate the characteristics of the Thomson-scattered radiation produced by the interaction of the simulated electron bunch and a counterpropagating laser pulse.

Here we will report the detailed estimation of the scattered-photon distribution in the case of Thomson scattering by a laser pulse and a counterpropagating electron bunch obtained by a particle in cell (PIC) simulation of laser wake-field acceleration with controlled particle injection by a sharp density transition [40]. We note that our physical conditions of the laser–plasma interaction are similar to those of Hafz et al. The sample particles we employed have been obtained by a PIC simulation, three dimensional in the fields and two dimensional in the coordinate, of the interaction between a 15-fs-long laser pulse of peak intensity $I = 2.5 \times 10^{18}$ W/cm^2 and a preformed plasma. The electron density of the plasma has a tailored profile presenting two plateaux separated by a steep transition. The produced electron bunch has mean energy about 10 MeV ($\langle\gamma\rangle = 20$) and remarkably low transverse and longitudinal normalized emittances $\epsilon_n^\perp = 0.1$ mm mrad and $\epsilon_n^\parallel = 2$ mm keV, respectively. The bunch is also very small, having transverse and longitudinal dimensions of 1 μm ($\sigma_T \simeq 0.5$ μm) and 3 μm ($\sigma_L \simeq 1.5$ μm), respectively, as shown in Fig. 13. We note, however, that the angular divergence $\Delta\theta_e \approx 100$ mrad is not fully satisfactory for linear Thomson backscattering quasi-monochromatic generation of soft X-rays, since $\Delta\theta_e\langle\gamma\rangle \simeq 2$.

We consider the scattering process of a flat-top pulse of energy $E_L = 5$ J, duration $T = 30$ fs, rise time $T_R = 6$ fs and wavelength 0.8 μm, interacting with the electron beam just outside the plasma region. The computation of the scattered-radiation distribution is performed, as in the former case, with the SALP formula by summing up the contributions of the
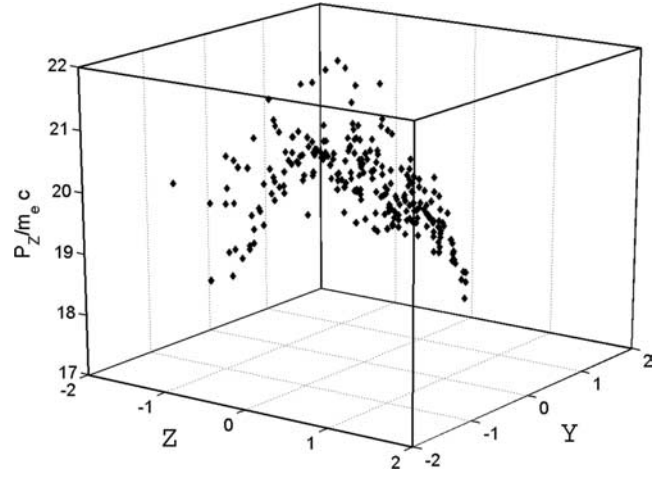

FIGURE 13   Longitudinal phase-space plot of the electron bunch obtained with a (3D in the fields and 2D in the coordinates) PIC simulation of laser wake-field acceleration with controlled trapping. The longitudinal and transverse sizes of the beam are about 3 μm and 1 μm, respectively, while the energy spread is about 5%

sample particles. In the linear regime ($w_0 = 100$ μm, $a_0 = 0.5$) the spectral distribution of the collected radiation within a scattering angle $\theta_{Max} = 0.5/\langle\gamma\rangle$ is very large, as was expected since the angular divergence of the bunch is comparable with θ_{Max} (see Fig. 14a, solid line). Reducing the collecting angle with $\psi = 0.3$ does not produce a narrower spectrum (solid dashed line) because the energy spread is dominated by the bunch angular divergence effect.

Since the transverse bunch size is so small, tightly focused beams can be safely employed and a fully nonlinear regime can be achieved with a pulse obtainable with present-day laser systems. We consider then further configurations in which the laser pulse is focused in a waist having $w_0 = 25$ μm (see Fig. 14b) with peak amplitude $a_0 = 2$, and $w_0 = 8$ μm (Fig. 14c) with peak amplitude $a_0 = 6$. In all the cases, the transverse inhomogeneity effects are negligible, since with $w_0 = 8$ μm we have $\sigma_0/w_0 \simeq 0.05$ and $\Delta\theta_e \ll [(1 - a_0^2/8\gamma_m^2)/(1 + a_0^2/8\gamma_m^2)](2w_0/cT) \simeq 1.6$ rad and $\theta_{TPF} \simeq 0.01$ rad.

Results of the computation in the fully relativistic ($a_0 = 2$ and $a_0 = 6$) regime show that narrow spectral distributions can be achieved even with such a large divergence bunch. The energy spread for the first harmonics reduced from about 50% with $a_0 = 0.5$ to 18% with $a_0 = 6$ (see Fig. 15 a and b). Moreover, tunability of the X-ray source can be easily obtained by changing the pulse energy/waist (and thus the pulse amplitude a_0) by taking advantage of the nonlinear red shift of the fundamental frequency.

4   Summary and comments

In this paper we have presented a comprehensive analysis of the scattered radiation produced by Thomson backscattering of a linearly polarized, flat-top and plane-wave laser pulse by a relativistic electron bunch presenting sizable angular divergence. Triggered by the results reported in Refs. [26–28], which dealt with pulses having a sharp flat-top profile, we have taken into account the effects of the rising front of the laser pulse on the particle dynamics for both the cases of sharp flat-top and smooth flat-top pulses.
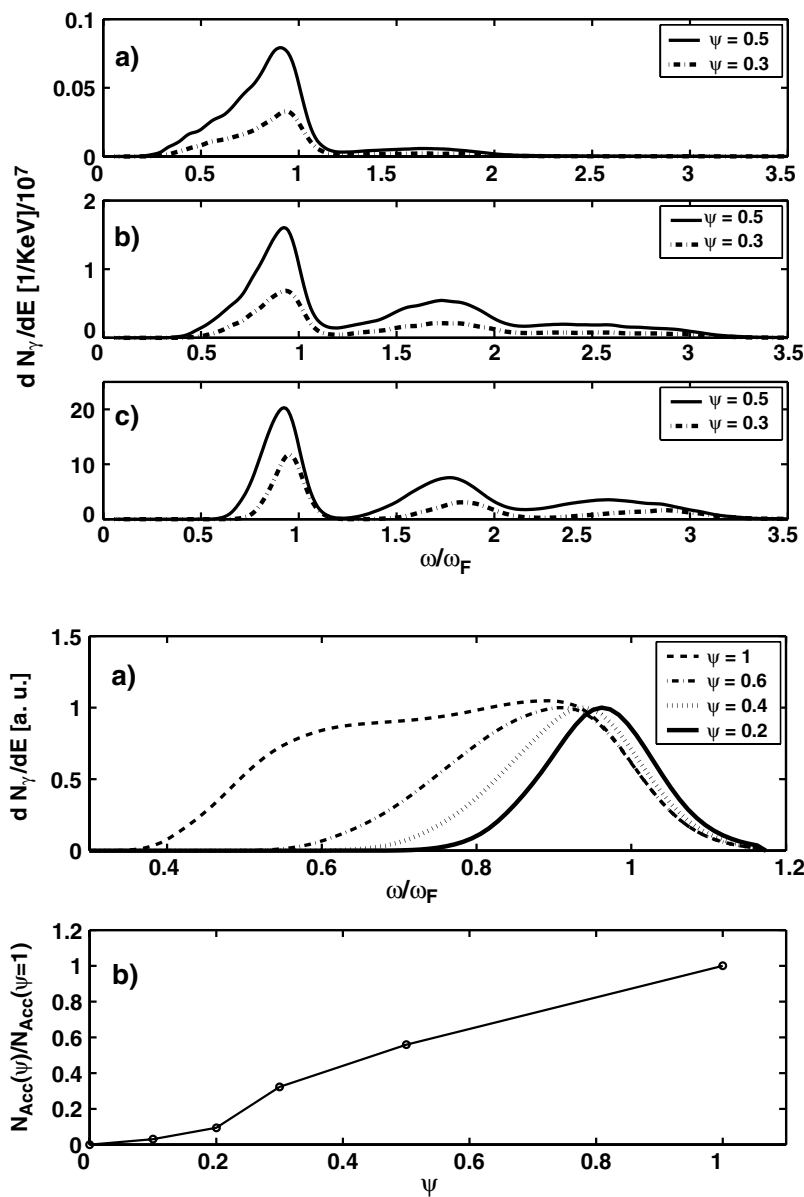
FIGURE 14 Backscattering of laser pulse with wavelength $\lambda_0 = 0.8\,\mu m$ delivering pulses of energy $E_L = 5\,J$ in $T = 30\,fs$ onto the electron bunch obtained with a 2D PIC simulation. Spectral distributions of the collected photons within the scattering angles $\theta_{Max} = \psi\sqrt{1 + a_0^2/\langle\gamma\rangle}$ with $\psi = 0.5$ (*solid line*) and $\psi = 0.3$ (*solid dashed line*). Results of the SALP computation for three laser pulse focalizations are reported. **a** $w_0 = 100\,\mu m\,(a_0 = 0.5)$; **b** $w_0 = 25\,\mu m\,(a_0 = 2)$; **c** $w_0 = 8\,\mu m\,(a_0 = 6)$. In the linear regime (**a**), due to the relatively large beam divergence, we obtain broad spectra by reducing ψ, too. In the full nonlinear regimes ((**b**) and (**c**)), however, a sizable reduction of the spectral broadening for the fundamental is found

FIGURE 15 Backscattering of laser pulse with wavelength $\lambda_0 = 0.8\,\mu m$, focused in a waist of size $w_0 = 8\,\mu m$ and delivering $E_L = 5\,J$ in $T = 30\,fs$, onto the electron bunch obtained with a 2D PIC simulation. **a** Normalized spectral distributions of the photons in the first harmonics collected within the scattering angles $\theta_{Max} = \psi\sqrt{1 + a_0^2/\langle\gamma\rangle}$ with ψ ranging from zero to unity (*solid line*) and $\psi = 0.3$ (*solid dashed line*). **b** Relative number of collected photons versus the acceptance normalized angle ψ

An analytical expression for the scattered-radiation distribution generated by a single particle having a small incidence angle has been derived in Sect. 1. Among the inclusion of the pulse rising front effects, our formulation differs from that of Ride et al. [29], since the scattered distribution is expressed directly in the laboratory coordinate system, with the possibility of using it directly to calculate the sum of contributions of the particles in a bunch. Several approximations have also been derived, the most useful for applications on RF-gun electron bunches being the small-angle in the long-pulse (SALP) limit, both in the linear and nonlinear regimes. Effects of the radial inhomogeneity of laser pulse amplitude have also been considered and *a posteriori* relations stating the validity of neglecting transverse ponderomotive forces have been clearly stated.

In Sect. 3 the *incoherent* radiation produced by an electron bunch was considered. In a linear regime, we presented a relation (see Eq. (53)) valid in the SALP limit, which looks different from an analogous relation presented in Ref. [8]. In particular, we found that the relation in [8] is an approximation of Eq. (53) valid in the case of scattering angles smaller than the beam divergence ($\theta_{Max} < \Delta\theta_e$). Useful relations valid in the linear case, involving the energy spread, the number of collected photons and the collecting acceptance angle, have also been reported.

Results of the simulations in the nonlinear regime showed that a sizable reduction of the scattered radiation energy spread for the fundamental harmonics is achievable for laser pulses in the full nonlinear regime ($a_0 \gg 1$). This effect is particularly evident for the case of Thomson backscattering from an electron bunch, which has been obtained with a PIC simulation of the LWFA with controlled injection, and having a large angular divergence $\Delta\theta_e\langle\gamma\rangle \simeq 2$.

We conclude by mentioning that very recently [41–43] the production of collimated and quasi-monochromatic relativistic electron bunches due to laser–plasma acceleration (but in a regime different from that reported in [40] and analyzed before) has been demonstrated by three independent experimental groups.

REFERENCES

1 D.G. Li, K. Yokoya, T. Hirose, R. Hamatsu, Jpn. J. Appl. Phys. B **42**(8), 5376 (2003)
2 C. Itzykson, J.B. Zuber, *Quantum Field Theory* (McGraw-Hill, Singapore, 1985)
3 F.R. Arutyunian, V.A. Tumanian, Phys. Lett. **4**, 176 (1963)
4 R.H. Milburn, Phys. Rev. Lett. **10**, 75 (1963)
5 C. Bemporad, R.H. Milburn, N. Tanaka, Phys. Rev. **138**, 1546 (1965)
6 M.D. Perry, G. Mourou, Science **264**, 917 (1994)
7 E. Esarey, S.K. Ride, P. Sprangle, Phys. Rev. E **48**(4), 3003 (1993)
8 P. Catravas, E. Esarey, W.P. Leemans, Meas. Sci. Technol. **12**, 1828 (2001)
9 J. Yang, M. Washio, A. Endo, T. Hori, Nucl. Methods Phys. Res. A **428**, 556 (1999)
10 K. Lee, Y.H. Cha, M.S. Shin, B.H. Kim, D. Kim, Phys. Rev. E **67**, 026502 (2003)
11 W.P. Leemans, C.E. Clayton, K.A. Marsch, C. Joshi, Phys. Rev. Lett. **67**(11), 1434 (1991)
12 I.C. Hsu, C.C. Chu, C.I. Yu, Phys. Rev. E **54**(5), 5657 (1996)
13 A.P. Potylitsyn, Phys. Rev. E **60**(2), 22 872 (1999)
14 P. Tomassini, M. Galimberti, A. Giulietti, D. Giulietti, L.A. Gizzi, L. Labate, Phys. Plasmas **10**(4), 917 (2003)
15 E. Esarey, Nucl. Methods Phys. Res. A **455**, 7 (2000)
16 H. Kotaki, M. Kando, H. Dewa, S. Kondo, T. Watanabe, T. Ueda, K. Kinoshita, K. Yoshii, M. Uesaka, K. Nakajima, Nucl. Instrum. Methods Phys. Res. A **455**, 166 (2000)
17 I.V. Pogorelsky, I. Ben-Zvi, T. Hirose, S. Kashiwagi, V. Yakimenko, K. Kusche, P. Siddons, J. Skaritka, T. Kumita, A. Tsunemi, T. Omori, J. Urakawa, M. Washio, K. Yokoya, T. Okugi, Y. Liu, P. He, D. Cline, Phys. Rev. ST Accel. Beams **3**, 090702 (2000)
18 M. Yorozu, J. Yang, Y. Okada, T. Yanagida, F. Sakai, S. Ito, A. Endo, Appl. Phys. B **76**, 293 (2003)
19 I. Sakai, T. Aoki, K. Dobashi, M. Fukuda, A. Higurashi, T. Hirose, T. Iimura, Y. Kurihara, T. Okugi, T. Omori, J. Urakawa, M. Washio, K. Yokoya, Phys. Rev. ST Accel. Beams **6**, 091001 (2003)
20 S.G. Anderson, C.P.J. Barty, S.M. Betts, W.J. Brown, J.K. Crane, R.R. Cross, D.N. Fittinghoff, D.J. Gibson, F.V. Hartemann, J. Kuba, G.P. LeSage, J.B. Rosenzweig, D.R. Slaughter, P.T. Springer, A.M. Tremaine, Appl. Phys. B **78**, 891 (2004)
21 A.Ts. Amatuni, M.L. Petrossian, Nucl. Methods Phys. Res. A **455**, 128 (2000)
22 E.G. Bessonov, A.V. Vinogradov, A.G. Tourianskii, Instrum. Exp. Tech. **45**(5), 718 (2002)
23 S. Ohtsuka, Y. Sugishita, T. Takeda, Y. Itai, J. Tada, K. Hyodo, M. Ando, Br. J. Radiat. **72**, 24 (1999)
24 K. Dobashi, M. Uesaka, A. Fukasawa, H. Iijima, J. Urakawa, T. Higo, M. Akemoto, H. Hayano, in *Proceedings of the EPAC02 Conference*, Paris, 2002
25 K. Takasago, A. Yada, T. Miura, M. Washio, F. Kannari, K. Torizuka, A. Endo, Int. J. Appl. Electromagn. Mech. **14**, 151 (2001)
26 F. He, Y.Y. Lau, D.P. Umstadter, R. Kowalczyk, Phys. Rev. Lett. **90**(5), 055002 (2003)
27 F. He, Y.Y. Lau, D.P. Umstadter, T. Strickler, Phys. Plasmas **9**(10), 4325 (2003)
28 Y.Y. Lau, F. He, D.P. Umstadter, R. Kowalczyk, Phys. Plasmas **10**(5), 2155 (2003)
29 S.K. Ride, E. Esarey, M. Baine, Phys. Rev. E **52**(5), 5425 (1995)
30 Y. Li, Z. Huang, M.D. Borland, S. Milton, Phys. Rev. ST Accel. Beams **5**, 044701 (2002)
31 J.D. Jackson, *Classical Electrodynamics* (Wiley, New York, 1975)
32 D. Giulietti, M. Galimberti, A. Giulietti, L.A. Gizzi, P. Tomassini, M. Borghesi, V. Malka, S. Fritzler, M. Pittman, K. Ta Phouc, Phys. Plasmas **9**, 3655 (2002)
33 T. Hosokai, K. Kinoshita, A. Zhidkov, K. Nakamura, T. Watanabe, T. Ueda, H. Kotaki, M. Kando, K. Nakajima, M. Uesaka, Phys. Rev. E **67**, 036407 (2003)
34 B. Quesnel, P. Mora, Phys. Rev. E **58**(3), 3719 (1998)
35 S.R. Amendolia, M.G. Bisogni, U. Bottigli, A. Ceccopieri, P. Delogu, G. Dipasquale, M.E. Fantacci, E. Lorenzini, A. Marchi, V.M. Marzulli, P. Oliva, R. Palmiero, M. Reggiani, V. Rosso, A. Stefanini, S. Stumbo, S. Tangaro, A. Venier, Nucl. Instrum. Methods A **461**, 428 (2001)
36 J.L. Coacolo, C. Pagani, L. Serafini, Nucl. Instrum. Methods A **393**, 430 (1997)
37 E. Esarey, R.F. Hubbard, W.P. Leemans, A. Ting, P. Sprangle, Phys. Rev. Lett. **79**, 2682 (1997)
38 S. Bulanov, N. Naumova, F. Pegoraro, J. Sakai, Phys. Rev. E **58**(5), R5257 (1998)
39 N. Hafz, H.J. Lee, J.U. Kim, G.H. Kim, H. Suk, J. Lee, IEEE Trans. Plasma Sci. **31**(6), 1388 (2003)
40 P. Tomassini, M. Galimberti, A. Giulietti, D. Giulietti, L.A. Gizzi, L. Labate, F. Pegoraro, Phys. Rev. ST-AB **6**, 121 301 (2003)
41 S.P.D. Mangles, C.D. Murphy, Z. Najmudin, A.G.R. Thomas, J.L. Collier, A.E. Dangor, E.J. Divall, P.S. Foster, J.G. Gallacher, C.J. Hooker, D.A. Jaroszynski, A.J. Langley, W.B. Mori, P.A. Norreys, F.S. Tsung, R. Viskup, B.R. Walton, K. Krushelnick, Nature **431**, 535 (2004)
42 C.G.R. Geddes, C. Toth, J. van Tilborg, E. Esarey, C.B. Schroeder, D. Bruhwiler, C. Nieter, J. Cary, W.P. Leemans, Nature **431**, 538 (2004)
43 J. Faure, Y. Glinec, A. Pukhov, S. Kiselev, S. Gordienko, E. Lefebvre, J.P. Rousseau, F. Burgy, V. Malka, Nature **431**, 541 (2004)